UfU
Independent Institute for
Environmental Issues

UfU-Paper #12/2025

Arne Reck, Tran Trung Cuong, Marlena Bodewein,
Moritz Floegel

CPEP 2 – Climate Protection through Energy Plants

Lam Dong Pilot Site Monitoring Report

Imprint

Independent Institute for Environmental Issues
Greifswalder Straße 4
10405 Berlin

T +49 (0)30 42 84 99 3-0
F +49 (0)30 42 84 99 3-59
info@ufu.de
www.ufu.de

Authors:
Dr. Arne Reck
Tran Trung Cuong
Marlena Bodewein
Moritz Floegel
12 | 2025

Supported by:

Federal Ministry
for the Environment, Climate Action,
Nature Conservation and Nuclear Safety

IKI INTERNATIONAL CLIMATE INITIATIVE

on the basis of a decision
by the German Bundestag

Table of Contents

Figures

Tables

List of Acronyms and Symbols

Symbol	Description	Unit
BD	Bulk density	g cm^{-3}
CEC_{eff}	Effective cation exchange capacity	meq $100g^{-1}$
CWSC	Cold-water soluble carbon	ppm
EC	Electrical conductivity	µS cm^{-1}
FC	Field capacity	Vol-%
HWSC	Hot-water soluble carbon	ppm
K_{K20}	Ionic potassium content	mg kg^{-1}
K_{sat}	Saturated hydraulic conductivity	cm h^{-1}
K_{tot}	Total potassium content	mg kg^{-1}
N_{NH4}	Cationic nitrogen content	mg kg^{-1}
N_{tot}	Total nitrogen content	mg kg^{-1}
P_{ava}	Cationic phosphorous content	mg kg^{-1}
POXC	Permanganate oxidisable carbon	ppm
P_{tot}	Total phosphorous content	mg kg^{-1}
pH_{H20}	Actual pH-Value	-
pH_{KCl}	Potential pH-Value	-
ST	Soil texture	mass-%
SOC	Soil organic carbon	%
SO_{4_dis}	Content of dissolved sulfate ions	mg kg^{-1}
SO_{4_tot}	Content of total sulfate ions	mg kg^{-1}
TAC	Total ash content	%
TM_{tot}	Pseudo-total trace metal content	mg kg^{-1}
TFC	Total fiber content	%
TLC	Total lipid content	%
TOC	Total carbon content	%
TPC	Total protein content	%

Symbol	Description	Unit
TStC	Total starch content	%
TSuC	Total sugar content	%
θ_{Field}	Gravimetrical field-water content	Vol-%

Acknowledgements

We gratefully acknowledge the Vietnam Coal and Minerals Industrial Group (VINACOMIN) for their longstanding support as part of the "CPEP – Energy Crops on Former Mining Sites" project series. Their invaluable assistance enabled the successful implementation of the initial CPEP project from 2015 to 2018 and the ongoing continuation project, "CPEP 2.

1 Introduction

Over the past three decades, Vietnam's rapid economic growth has significantly increased energy demand. The country's energy mix remains dominated by fossil fuels – coal, oil, and natural gas – leading to serious environmental challenges and contributing to climate change. However, renewable energy sources such as wind, hydropower, biofuels, and waste-to-energy have gained prominence, with high expansion potential due to favourable geographic and climatic conditions. Biofuels, in particular, play a stabilising role by providing storable, locally available energy when wind or solar power is unavailable. They also reduce greenhouse gas (GHG) emissions compared to fossil fuels.

To promote renewable energy, the Vietnamese government has enacted policies such as mandatory bioethanol blending. Yet, expanding energy crop production can drive land-use change, including deforestation, and compete with food production, potentially raising food prices and threatening food security. Moreover, arable land is diminishing due to urbanisation and soil degradation, heightening the need for sustainable bioethanol production alternatives.

From 2015 to 2018, the pilot project "Climate Protection through Energy Plants (CPEP)" successfully demonstrated that sustainable energy crop cultivation on former mining sites in Vietnam can mitigate competition for land between renewable biomass and food production. The project also showed how such practices can lessen negative land-use impacts and support climate protection efforts. Three pilot sites located in northern and southern Vietnam were used to identify suitable energy crop systems for post-mining landscapes.

The second phase, CPEP2, builds on these findings by implementing targeted measures to refine, expand, and detail the results achieved so far. Its goal is to develop concrete recommendations for large-scale application of the CPEP approach. A central activity involves the detailed monitoring of the experimental site in Lam Dong Province, demonstrating the suitability of cassava as a bioethanol feedstock and its performance in recultivation on a pilot scale. Monitoring includes detailed soil investigations together with qualitative and quantitative biomass investigation of the cassava harvest.

By cultivating energy crops on former mining sites – lands often unsuitable for food production due to poor soil quality and heavy metal contamination – CPEP offers mining companies a sustainable recultivation solution and an opportunity to generate additional income through the sale of cassava to bioethanol producers. This approach not only supports Vietnam's renewable energy goals but also promotes environmental restoration and economic resilience in post-mining regions.

1.1 Objectives of the Monitoring of the Pilot Site in Lam Dong Province

The second phase of the Climate Protection through Energy Plants (CPEP 2) project involves the cultivation of cassava and VA06 gras on pilot scale accompanied by an intensive monitoring of the recultivation performance based on selected ecological variables. Located in Lam Dong Province in central Vietnam, the site is now left bare and was agriculturally cultivated between 2022 and 2024. The monitoring programme focuses on analysing standard soil physicochemical parameters, trace metal content in the soil and in the cassava plants, carbon quality analysis and soil erosion. Based on these data, the study pursues the following key objectives:

1. Contaminant Risk Assessment: Evaluation of the potential transfer of contaminants via the soil-plant and soil-groundwater pathways.

2. Qualitative Assessment of Ecosystem Services: Description and analysis of the ecosystem services provided by energy crop cultivation on post-mining land.

3. Feasibility of Energetic Utilisation: Assessment of the suitability of planted Cassava for bioethanol production.

Through these objectives, CPEP 2 aims to assess the medium- and long-term viability of selected energy plant systems for the recultivation of post-mining sites in Vietnam, as well as their qualitative benefits of these systems for ecosystem services. The findings will inform the development of management recommendations for soil protection and sustainable land-use practices on similar sites across Vietnam.

2 Methods

2.1 Site description

The study area is situated within the Tang Rai mining area located in Bao Lam District, Lam Dong Province, approximately 180 km north of Ho-Chi-Minh City (Figure 1). While parts of the mine remain operational, the experimental site is established on a former bauxite open-pit mine. Prior to mining, the upper soil layers were removed and stored adjacent to the site. Following the cessation of mining activities, a 50 cm layer of stored topsoil, enriched with compost substrate, was reapplied to the area before planting

The region exhibits a mountainous midland topography, defined by steep slopes, river- and stream-intersected valleys, and elevated flat plateaus. The near-surface geology is predominantly of basaltic volcanic origin (Hoang, et al., 2019). This volcanic substrate has undergone extensive weathering, resulting in a lateritic crust of Pleistocene age, with reported thicknesses ranging from 20-26 m. Within this weathered profile, bauxite deposits have developed, typically occurring as banks 1-12 m thick (Phuong, 2015). Valley floors are characterized by alluvial sediments, reflecting ongoing fluvial processes. Within the valleys sediments of alluvial origin dominate. The dominant soil type in the study area is Ferralsol, derived from the weathering of basaltic parent material (Cuong, et al., 2025). Ferralsols are noted for their deep, highly weathered profiles, which are rich in clay, exhibit low natural fertility, and are strongly acidic. These soils are typical of tropical and subtropical environments, where intense weathering and leaching processes have removed soluble minerals, leaving behind iron and aluminium oxides that contribute to their distinctive red or yellow hues.

The climate of Bao Lam is classified as Am (Tropical Monsoon Climate) according to the modified Köppen-Geiger system. The area experiences an average annual temperature of 23.0°C, with April being the hottest month (29.4°C) and January the coldest (15.8°C). Annual precipitation averages 3,370 mm, with a distinct rainy season from April to October and a dry season in the intervening months (Brömme, et al., 2018).

In March 2021, the experimental site was prepared by application of a 24-35 cm layer of topsoil mixed with compost to level the surface. However, approximately 100 m_2 at the boarder of Plot 14 remained untreated (cf. Figure 1). A perimeter trench and fence were installed to prevent livestock browsing. Additionally, an irrigation system with a 40 m^3 capacity was set up.

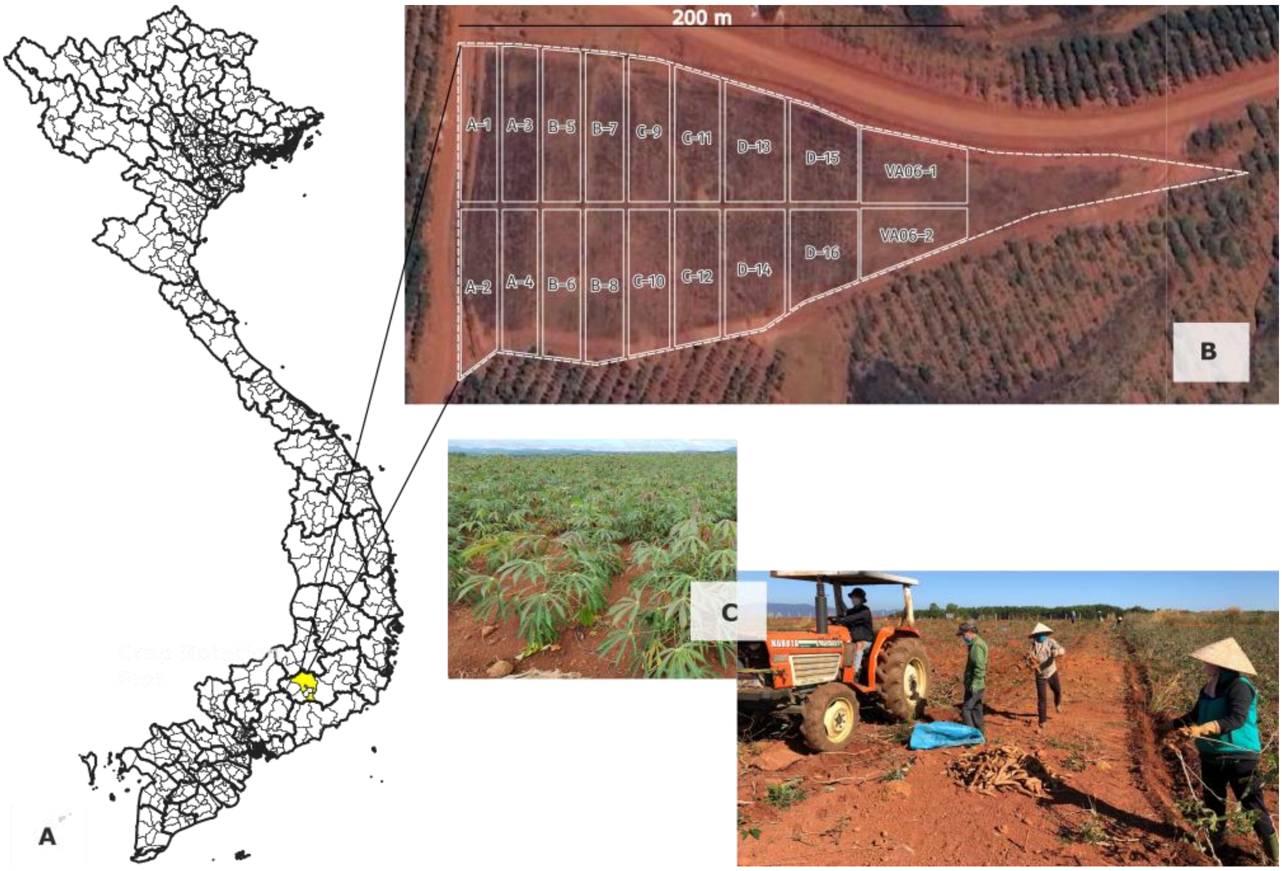

Figure 1: (a) Location of the experimental site within the Bao Lam District, Lam Dong Province, (b) areal image of the experimental site with the plot divisions, (c) cassava plantation and cassava harvest in January 2022.

2.2 Experimental Design

2.2.1 Planting and Harvest

Cassava cuttings of variety KM140 were sourced from the Hung Loc Agricultural Research Center, Trang Bom, Dong Nai (Table 1). The study site was a former mining area with poor soil quality. Cassava was planted at a density of 13,000 plants per hectare, with a spacing of 1.1 m × 0.7 m. The experimental site was ploughed twice, and rows were slit 1.1 m apart. Microbial organic fertiliser and phosphate fertiliser were applied directly to the trenches. Cassava cuttings, 25-30 cm in length (each with 3-4 eyes), were planted horizontally in the trenches and buried 3-4 cm below the soil surface. To prevent viral and fungal infections, cuttings were pre-treated by soaking in Gaucho 600FS solution (0.016% concentration) for 5 minutes. Planting occurred on April 9, 2021, followed by mung bean sowing on April 11, 2021. After treatment, new leaves exhibited the variety's characteristic red-purple coloration, and plants averaged 30-35 cm in height with 13-15 leaves. At 50 days, a second fertilizer application (250 kg urea, 250 kg KCl, 20 kg $ZnSO_4$) was combined with composted organic fertiliser and bed raising (7-10 cm). Black beans were sown between cassava rows to provide organic biomass, though survival was below 10%. By 100 days, cassava plants reached 60-70 cm, with flowering and branching observed. Lower leaf yellowing indicated nutrient deficiency, addressed with the application of 400 kg NPK

Fertilizer application per hectare included:

- 5 tons of manure (not composted at planting)
- 160N–80P_2O_5–160K_2O
- Superphosphate: 500 kg
- Urea: 350 kg
- Potassium: 400 kg
- NPK (16:16:16): 300 kg

Initial cassava growth exceeded 90%, while mung bean germination reached 97% within 10 days. However, due to hot, dry conditions and incomplete irrigation, mung bean survival dropped to 10–12%. Cassava growth was slow, with plants averaging 7-10 cm in height and 5-6 pale leaves 26 days after planting. About 1% of plants showed viral symptoms (e.g., curly leaves, leaf mosaic). The first fertiliser application (250 kg urea and 250 kg potassium) was made 26 days after planting. Infected plants were removed and replaced. Zinc deficiency was observed 40 days after planting, treated with a foliar spray fertiliser on August 5. Cassava growth ceased at 225 days, with leaf fall and fruit development (10 fruits per plant). Harvest was conducted in mid-January 2022. However, 3,000–4,000 m^2 of the 1.6 ha plot exhibited poor growth, particularly in Plots 4, 6, 8, 10, 12, and 14, with Plots 10 and 12 most affected. These areas lost most leaves by 185-195 days, retaining only 2-3 upper leaves, significantly reducing yield. Harvest occurred on January 15-16, 2022 (Figure 1c). Survival rate was 90%, but actual yield was lower than expected due to theft (30% of plants), hard soil impeding uprooting, and improper harvesting techniques causing root breakage.

VA06, a local cultivated variety of *Pennisetum purpureum* (Elephant grass or Napier grass), is a fast-growing C4 grass capable of reaching heights of 3-7 m. Under favourable conditions, the plant can grow several meters within 60 days. Its deep root system, extending 3-4 m in length and up to 2.5 m in diameter, confers significant drought resistance. VA06 is valued for its high productivity on low-fertility sites, resistance to common pests and diseases, and effectiveness in erosion control. While primarily cultivated for silage production, it also serves as a feedstock for biogas production and livestock feed. VA06 grass was propagated from 4-5-month-old stems measuring 1.5-1.8 m in height and planted in rows spaced 1.1 m apart, with 0.3 m between individual plants. Initially, VA06 exhibited poor growth due to nutrient deficiency, prompting the application of fertiliser. Following fertilisation, the survival rate improved to 95-100%, with normal growth and development observed from planting to the present. VA06 has not been harvested systematically during the monitoring period, as it was maintained for wind and water erosion control.

Mung beans were selected and intercropped with cassava to provide rapid soil cover and additional nutrients, leveraging the legume's nitrogen-fixing qualities. The mung bean varieties were sourced from neighbouring areas to facilitate transportation and ensure adaptation to local climate and soil conditions.

Vetiver grass, known for its massive root system that penetrates up to 3 m deep, is typically planted on slopes and roadsides to prevent soil erosion. When planted densely, vetiver forms a protective barrier that mitigates floods and reduces sediment erosion. It is particularly suited to marginal soils containing heavy metals, as it can absorb contaminants such as arsenic, cadmium, mercury, lead, nickel, copper, and chromium. Vetiver cuttings were propagated by dividing branches, ensuring each cutting had 2-3 roots. These cuttings were planted along the perimeter of the test sites and around the irrigation reservoir. However, due to insufficient watering during periods of hot, dry weather, the vetiver cuttings experienced a 0% survival rate.

Table 1: Selected plants for the Lam Dong experimental site and their application.

Characteristic	Cassava	VA06	Mung beans	Vetiver
Area	1.6 ha	0.4 ha	1.6 ha	Planted on the banks of ditches
Seed	KM140	Local	Local	Local
Planting time	9-10/4/2021	5/5/2021	11/4/2021	5/9/2021
Density	13,000 plants ha^{-1}, 1.1 x 0.7 m	1.1 x 0.3 m	-	-
Supplier	Hung Loc Agricultural Research Centre	Local	Local	Local

2.2.2 Soil Sampling

The whole experimental site (1.6 ha) was subdivided into four cassava plots (A-D) and two VA06 plot (Figure 1b), each measuring approximately 1,00 m^2. To determine the soil chemical parameters and trace metal contents, ten soil samples were collected from the upper soil layer (0-30 cm depth) per plot (Figure 2c, orange dots). These samples were combined into a single composite sample for analysis. Sampling was performed using core drills to minimize contamination from the litter layer. All soil samples were stored in polyethylene bags until laboratory analysis.

For soil physical property investigations, undisturbed core samples were collected at one location per plot at two depth intervals, 0-15 cm and 16-30 cm, resulting in two undisturbed samples per plot (Figure 2c, blue dots).

Soil sampling campaigns occurred in multiple years with the following scope:

- 2021: Soil status quo analysis for all three plots of the experimental site (full set of standard physical and chemical parameters as listed in Table 2)
- 2022: Soil status quo analysis after first cassava planting cycle (full set of standard physical and chemical parameters as listed in Table 2)

- **2023:** Simplified soil status quo analysis prior to second cassava planting cycle (only full set of standard chemical parameters as listed in Table 2). Detailed analysis of bioavailability of trace metals (in situ soil solution sampling with suction cups and sequential extraction in the laboratory; cf. below). Detailed analysis of soil hydrological parameters, as described below.

- **2024:** Detailed analysis of soil organic carbon, as described below.

In April 2023, two reference profiles were excavated on the experimental site. Disturbed soil samples were collected from the upper (0-30 cm) and lower (30-50 cm) layers. From the same layers, three undisturbed soil samples were taken to analyse soil hydrological properties, including soil water retention and saturated water conductivity (K_{sat}). In 2024, two reference profiles were excavated again on the experimental site following the same procedure as in the 2023 campaign with samples collected from the upper (0-30 cm) and lower (30-50 cm) layers. This approach enabled a qualitative assessment of soil carbon stability and hydrological function.

Suction cups to sample soil solution were installed close-by the reference profiles of the 2023 campaign at depths of 30 cm. Each plot received two suction cups, resulting in 4 cups in total for the experimental site. Installation involved drilling narrow holes with a hand auger and adding slurry to improve soil-cup contact. Suction was applied using a glass bottle and a hand pump. To avoid contamination, the first sample was discarded after 24 hours. Subsequent samples were collected every 24 hours over three

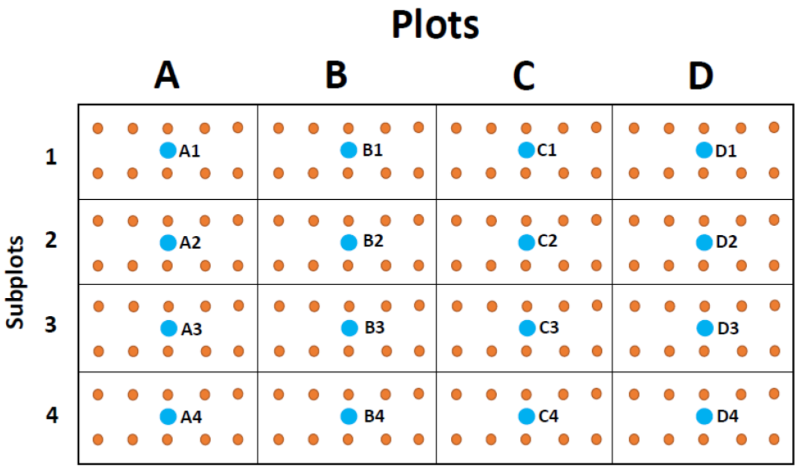

Figure 2: Exemplary sketch of 1.6 ha experimental site in Lam Dong with the subdivision into five equal-sized plots of 1,000 m² each and sampling points for chemical (orange dots) and physical (blue dots) analysis.

consecutive days, yielding six samples per plot. Soil solution was transferred to centrifuge bottles, acidified with nitric acid (HNO_3) for stabilization, and stored for laboratory analysis. Glass containers were cleaned with distilled water between samples. Sampling occurred at the end of the dry season, shortly after cassava planting. To ensure uniform conditions, we simulated irrigation by watering the soil around each suction cup with tap water (approximately 5 l per cup daily) for the first four days.

2.2.3 Laboratory Measurements

The methods applied to determine the soil's physical and chemical properties on composite and undisturbed samples are summarised in Table 2. Table 3 shows the parameters analysed for the harvested Acacia trees. Prior to laboratory analysis, the acacia samples were crushed. Soil water retention properties and saturated hydraulic conductivity (K_{sat}) were analysed at VNUA, Hanoi, following DIN EN ISO 11274 (2014). Additional high matric potential data (>pF 3) were measured on disturbed samples using a WP4C device. Soil water retention measurements for pF >3, the soil organic carbon fraction analyses and the sequential extraction of trace metals (see description below) were conducted by the University of Cologne, Germany, in their laboratory. All other measurements, as well as the respective sample preparation for the 2021 and 2022 campaigns, were conducted by the Soil and Fertiliser Research Institute, an ISO-certified laboratory in Hanoi. Unless stated otherwise, all laboratory measurements were conducted in accordance with the Technical Standards in Vietnam (TCVN). In cases where no Vietnamese standard exists, other internationally accepted measurement techniques were applied.

To analyse the mobile and readily bioavailable fraction, the first two steps of the sequential extraction procedure described by Zeien & Brümmer (1989) were performed. Step 1 involved extracting the soil sample with 1 M ammonium nitrate (NH_4NO_3). One gram of sieved (<2 mm) soil was weighed into a 50 ml centrifuge tube, and 25 ml of NH_4NO_3 solution was added. The suspension was shaken for 24 hours on a horizontal shaker, then centrifuged for 10 minutes at 4,000 rounds per minute. The supernatant was filtered through a 0.45 µm cellulose filter, stabilised with nitric acid (HNO_3), and analysed using ICP-OES. Step 2 utilised ammonium acetate (NH_4OAc) at pH 6. The pellet from Step 1 was resuspended in 25 ml of NH_4OAc, shaken, centrifuged, and filtered as described above. Subsequently, 12.5 ml of NH_4NO_3 was added to the pellet, manually shaken, and centrifuged again for 10 minutes at 4,000 rpm. The supernatant was filtered through a 0.45 µm filter, combined with the NH_4OAc extract, stabilised with HNO_3, and analysed by ICP-OES. For external validation, the entire procedure was repeated, and the extracts were submitted to the Federal Institute for Geosciences and Natural Resources (Germany) for analysis via ICP-MS. Prior to analysis, samples were additionally filtered through a 0.2 µm cellulose.

Table 2: Soil physical and -chemical laboratory techniques as well as the corresponding standards.

Parameter/Description	Method	Standard
	Standard physical and chemical soil parameters	
BD Bulk density	Drying at 105 °C until constant weight	TCVN 6860:2001
ST Soil texture	Wet sieving and sedimentation analysis	TCVN 8567:2010
FC Field capacity	Gravimetrically determined water content of a previously saturated soil sample in equilibrium under free draining conditions	Blažka and Fischer (2014)

Parameter/Description	Method	Standard
θ_{Field}	Gravimetrically determined water content	-
pH_{H2O} and pH_{KCl} pH value	Potentiometric pH determination	TCVN 5979:2007
EC Electrical conductivity	EC sensor	TCVN 6650:2000
K_{tot} and K_{K2O} Total and ionic potassium content	Colorimetrical determination in suspended soil	TCVN 8940:2011, TCVN 8660:2011
N_{tot} and N_{NH4} Total and cationic nitrogen content	Modified Kjeldahl method (sulfuric acid digestion followed by adding sodium hydroxide, production ammonium of all nitrogen species and subsequent titration to determine total N/distillation with natrium hydroxide and subsequent titration to determine ammonium-N contents	TCVN 6498-1999, TCVN 5255:2009
P_{tot} and P_{ava} Total and available phosphorus content	Colorimetric determination in solution, sulphuric and perchloride acid digestion of soil sample for determining total phosphorous, Bray No 2 solution for extraction of adsorbed forms of phosphate only	TCVN 8940:2011, TCVN 8942
SO_{4_tot}, SO_{4_dis} Contents of total and dissolved sulphate ions	Gravimetrical determination by adding barium chloride and weighting the precipitate of barium sulphate	TCVN 6656:2000
CEC_{eff} Effective cation exchange capacity	Determination of the content of exchangeable sodium, potassium, calcium, and magnesium in soil using barium chloride solution	TCVN 6646:2000
SOC Soil organic carbon	Walkley-Black Method (chromic acid wet oxidation of soil organic carbon)	TCVN 8941:2011
TM_{tot}[‡] Pseudo total trace metal content [‡]	Aqua regia digestion followed by ICP-OES spectrometry (Inductively coupled plasma with optical emission spectrometry) except for Mercury (Cold-vapor atomic spectrometry or	TCVN 8246:2009, TCVN 6496, TCVN 8882;

Parameter/Description	Method	Standard
	cold-vapor atomic fluorescence spectrometry)	
	Soil organic carbon quality and soil hydrological parameters	
CWSC, HWSC, POXC Cold-water soluble carbon, hot-water soluble carbon and permanganate oxidisable carbon	Fractions belonging to the labile pool of soil organic carbon with typical turnover times from 20-100 days	-
Soil water retention	Relationship between the soil water content (ϴ) and the soil water potential (pF)	following DIN EN ISO 11274 (2014)
K_{sat} Saturated hydraulic water conductivity	Measurement of how easily water can move through fully saturated soil pores, representing the soil's ability to transmit water under saturated conditions	-

‡ Following trace elements were determined per soil sample: Al, As, B, Ba, Be, Bi, Cd, Co, Cr, Cu, Ga, Hg, K, Li, Mn, Mo, Na, Ni, Pb, Sb, Se, Sn, Sr, Ti, Tl, V, Zn, Fe, Ca, Mg

Table 3: Laboratory techniques applied to investigate the chemical *Acacia* properties.

Parameter/Description	Method	Standard
WD_{plant} Plant dry mass	Drying at 60-70°C until constant weight	10TCN 842:2006
TOC Total carbon content	Dry combustion at 1,200°C	-
TM_{tot}‡ Pseudo total metal content ‡	ICPE-OES spectrometry (Inductively coupled plasma with optical emission spectrometry) except for Mercury (Cold-vapor atomic spectrometry or cold-vapor atomic fluorescence spectrometry)	TCVN 8246:2009, TCVN 6496:2009, TCVN 8882:2011
TStC Total starch content	Ewers polarimetric method (one portion is hydrolysed with dilute hydrochloric acid; other portion is treated with 40 % (V/V) ethanol to	TCVN 9935:2013

Parameter/Description	Method	Standard
	extract soluble sugars and polysaccharides)	
TSuC Total sugar content	Dissolution in potassium permanganate and subsequent titration	TCVN 4074:2009
TFC Total fiber content	Tea Method for determination of the crude content (boiling with sulfuric acid and sodium hydroxide followed by washing with hydrochloride acid)	TCVN 5714:1993
TPC Total protein content	Kjeldhal method (Sulfuric acid digestion followed by distillation and subsequent titration)	TCVN 10791:2015
TLC Total lipid content	Kjeldhal method (Sulfuric acid digestion followed by distillation and subsequent titration)	TCVN 8125:2009
TAC Total ash content	Incineration at 500-1,000°C	TCVN 8124:2009

‡ Following trace metals were determined per Acacia sample: Ag, Al, B, Ba, Be, Bi, Cd, Co, Cr, Cu, Fe, Ga, Hg, K, Li, Mn, Mo, Na, Ni, Pb, Sb, Se, Sn, Sr, Ti, Tl, V, Zn

2.3 Ethanol Capacity

To evaluate the bioethanol-production potential from the cassava harvested at the Lam Dong experimental site, the ethanol capacity was determined at the laboratory of the Hanoi Open University in 2022. Cassava tubers were harvested and peeled on-site. Fresh cassava was divided into two batches: one batch (2 kg) was dried and ground, while the other (2 kg) was used fresh. For drying, cassava roots were sliced into 0.5 cm thick pieces and dried in an oven at 90°C for 3 hours. Water content was determined by further drying at 105°C for 5 hours.

α-Amylase (100,000 U mL^{-1}) and glucoamylase (260,000 U mL^{-1}) were purchased from Angel Yeast Co. Ltd. Yeast culture was prepared in YMB media (Yeast extract 0.3%, Malt extract 0.3%, Peptone 0.5%, Glucose 1%). Cassava powder was gelatinised in 0.1 M phosphate buffer (pH 5.0) at 100°C for 5 minutes. α-Amylase was added at 5,000 U g^{-1} dried cassava and incubated at 90°C for 3 hours. After cooling to 60°C, glucoamylase was added at 15,000 U g^{-1} dried cassava and incubated at 60°C for 1.5 hours (Wangpor, et al., 2017). The hydrolysate was then adjusted to 4 L with water. Ethanol fermentation was conducted in a 10 L fermenter. *Saccharomyces cerevisiae* seed culture was prepared in YMB media at 30°C, 200 rpm for 24 hours. 80 mL of seed culture was inoculated into 4 L of cassava hydrolysate. Fermentation was carried out at 30°C, 50 rpm, without aeration for 72 hours.

The reduced sugar was determined using Miller's method with DNS reagent (Miller, 1959). The ethanol content was measured by the density method (TCVN 8008:2009) after cooling the sample to 20°C. Finally the fermentation efficiency was calculated by the following equation:

$$E_{fermentation}(\%) = \frac{m_{yielded\ ethanol}}{m_{theorethical\ etahnol}} * 100$$

2.4 Soil Water Modelling

Soil water fluxes were simulated using the HYDRUS-1D model, a widely used numerical tool for analysing variably saturated water flow and solute transport in porous media (Šimůnek, et al., 2008). The model allows for detailed representation of soil profiles, boundary conditions, and plant-water interactions, making it suitable for assessing water balance and solute dynamics in agricultural and post-mining soils. The soil profile was discretised into two layers (0-25 cm and 25-200 cm depth), with a total of 200 nodes and increased node density near the boundaries to improve simulation accuracy. Simulations were run for a two-year period, with the first year serving as a spin-up phase to achieve numerical equilibrium. The upper boundary condition was defined by atmospheric forcing, including precipitation and evapotranspiration, while the lower boundary was set to free drainage, assuming a water table depth >10 m. Daily precipitation data were sourced from the Bao Loc meteorological station. Potential evapotranspiration (ET_0) calculated with the Penman–Monteith equation, was retrieved from a global data set provided by Singer et al. (2021). Cassava crop dynamics were parameterised using a leaf area index (LAI) series derived from Phoncharoen et al. (2019). Canopy radiation extinction was set to 0.57 (Mwamba, et al., 2021). Root distribution was set to 50 % at surface and decreased linearly to the field-observed maximum rooting depth of 40 cm. The root water uptake parameters were set according to Feddes (1978) with default values for potatoes to parametrise the water stress response function. Soil hydraulic properties were derived from retention data (see previous section).

2.5 Soil Erosion Modelling

A digital elevation model (DEM) was generated for erosion modelling using a DJI Mini 2 drone. The test site was surveyed at a flight altitude of 30 meters, with images captured approximately every ten meters to ensure sufficient overlap (Figure 3a). Overlapping images are necessary to guarantee that each point on the ground is photographed from multiple perspectives. The collected images were processed using Agisoft Metashape Professional (Version 2.1.0 build 17532) to create the DEM (Figure 3b and c). Due to computational restrictions, the received DEM resolution (1.07 x 1.07 cm pixel^{-1}) was downscaled to 20 x 20 cm pixel^{-1} in QGIS.

Erosion and erosion pathways were estimated using the QNSPECT plugin for QGIS, developed by the NOAA Office for Coastal Management (2022). This plugin applies the Universal Soil Loss Equation (USLE) after Wischmeier & Smith (1978) to assess soil erosion. The following input layers were prepared for the analysis:

- **Land Cover Raster:** This layer provides information on land cover types and associated soil properties. For the experimental site, the land cover was classified as "Cultivated Crops" and "Bare Soil" for comparison based on the classification scheme provided by NOAA (Office for Coastal Management, 2024).
- **Digital Elevation Model (DEM):** Derived from drone imagery, this layer supplies data on slope and test area dimensions.
- **Hydrological Soil Group Raster:** This layer classifies soil according to the NRCS Curve Number (U.S. Department of Agriculture, Soil Conservation Service, 1986). The soils in Lam Dong were identified as class B soil (silt-loam or loam).
- **Rainfall and Runoff Raster:** The erosive impact of rainfall is a critical factor in erosion modelling. For the R-factor, data from the Global Rainfall Erosivity Database (GloREDa) (Panagos, et al., 2017; Panagos, et al., 2023) was used. The interpolated R-factor for Lam Dong is 9,686 MJ mm ha^{-1} h^{-1} yr^{-1}.
- **Soil Erodibility Raster:** This factor represents the soil's susceptibility to erosion, which depends on local soil properties. Soil data were derived from field observations and classified as silt loam, with equals a K-factor of 0.36.

The Universal Soil Loss Equation (USLE) in the version by Wischmeier & Smith (1978), estimates soil due to rainfall using the following equation:

$$A = R * K * L * S * C * P$$

With A = calculated soil loss per unit area, R = Rainfall and runoff factor, K = Soil erodibility factor, L = slope length factor, S = Slope steepness factor, C = Cover and management factor, and P = support practice factor.

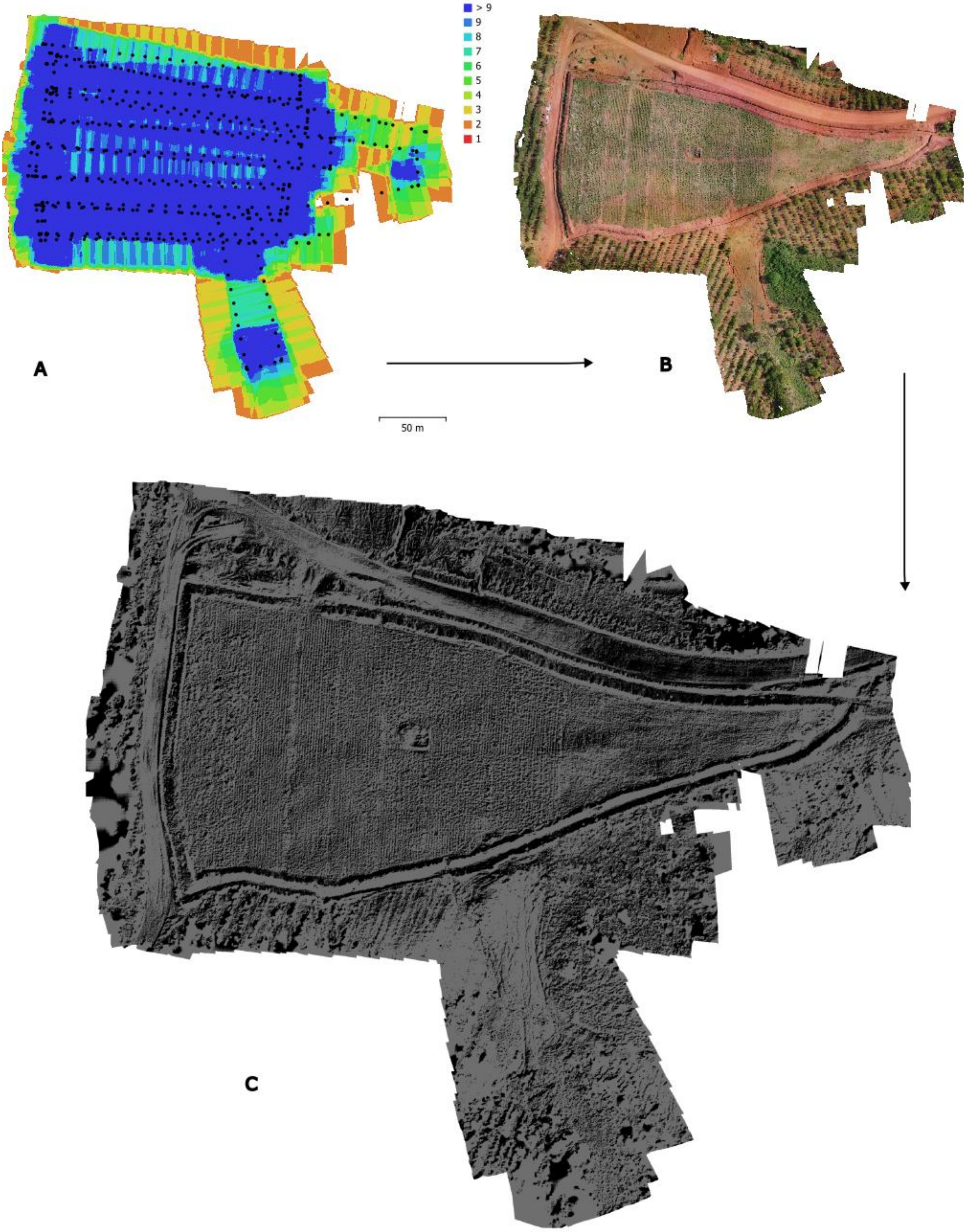

Figure 3: Workflow illustrating the process of deriving a digital elevation model (DEM) for the experimental site: (a) drone imaging, showing camera locations and image overlap; (b) the resulting high-resolution aerial image; and (c) the DEM calculated from the drone imagery.

2.6 Data Management

All field and laboratory results passed the following steps of data analysis:

- Data cleansing: elimination of incorrect data points; definition of consistent handling for incomplete datasets; checking for duplicate datasets;
- Data validation: checking for realistic value ranges; identification of outliers and definition of consistent validation rules;
- Data exploration: univariate and multivariate analysis using descriptive statistics.

3 Results

3.1 Soil Status Quo 2020/2022/2024

3.1.1 Physicochemical Standard Parameters

Soil texture analysis reveal silt as the dominant texture fraction in all samples (Figure 4) with only little variation between individual samples. The sand fraction only covers between 10-20%. Clay as the other fine fraction is negligibly low and covers less than <10% in all samples. Accordingly, soil texture at the study site only covers the soil textural class of Silt Loam. This means, in turn, the soil contains an unbalanced mixture of silt, sand and clay and the silt fraction clearly dominates the soil properties. Based on these soil textural analysis the main soil properties can summarized as follows:

- Granular or crumb-like structure in dry conditions, shifting to form a weak ribbon when moist, which indicates moderate cohesion
- Moderate compaction risk that significantly increases with wet soil conditions
- Good drainage and water holding capacity
- Moderate soil fertility due to the moderate nutrient retention by the silt fraction (moderate cation exchange capacity, see also Section 3.1.2 (Page 18)

At the beginning of site recultivation, the average soil organic carbon (SOC) content across the entire experimental field was 2.60 ± 0.73 mass-% (Figure 5). During the first planting cycle, all sub-plots experienced a slight decline in SOC, reaching an average of 2.25 ± 0.55 mass-% by 2022. In the second planting cycle, however, SOC levels rose again to 2.72 ± 0.61 mass-% in 2023. When considering the

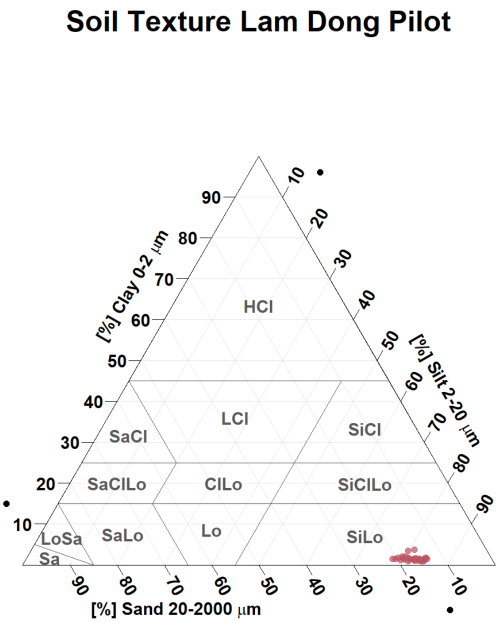

Figure 4: Soil texture triangle for the Lam Dong pilot site. The soil textural classes correspond to the International Union of Soil Sciences system (IUSS Working Group WRB, 2022). The plotted values are derived from composite samples of depths between 0-30 cm (n = 32).

entire investigation period from 2021 to 2023, SOC increased on average across all sub-plots. Spatial variations in SOC were evident among the sub-plots. Sub-plot C consistently showed lower SOC levels (2.01 ± 0.45 mass-%), while sub-plot D had significantly higher values (3.03 ± 0.59 mass-%) compared to the field average. By contrast, bulk density (BD) remained stable, with values of 1.06 ± 0.10 g cm^{-3} in 2021 and 1.07 ± 0.08 g cm^{-3} in 2022. BD measurements were not continued in 2023 due to the interruption of the second planting cycle. The minimal change in BD over this short period is expected, as the re-development of soil structure typically requires several years. Both SOC and BD values fall within the ranges commonly reported in the literature for Ferralsols in Vietnam (2.22 ± 0.70 mass-% for SOC and 1.02-1.09 g cm^{-3} for BD) (Ha, 2010). This is notable, given the site's history of mining activities and associated soil disturbances.

Considering all sup-plots and all monitoring years, the pH-value ranges from moderately to strongly acidic (Figure 5). However, if we consider the pH value measured in H_2O, which more accurately reflects the pH experienced by plants in the soil solution, a decrease is observable for all sub-plots (from 5.71 ± 0.17 in 2021 to 5.29 ± 0.11 in 2023). Although soil pH measured in a water suspension more accurately reflects current soil conditions, this value is highly sensitive to changes in boundary conditions, such as fertiliser application and rainfall, and is therefore prone to seasonal variations. A more reproducible measure of soil acidity is the pH value measured in potassium chloride (KCl), as this value is less affected by short-term or seasonal changes in the composition of the soil solution. Considering this value, the pH of both plots changed marginally, from 5.31 ± 0.08 to 5.14 ± 0.11 in 2023. In summary, the nearly stable soil pH value determined in potassium chloride suggests that different seasonal boundary conditions are a plausible cause of the lower pH observed in the 2022 and 2023 campaigns compared to the 2021 status quo. Nevertheless, other causes remain possible, as the reduced pH (H_2O) in both plots may reflect an increase in SOC due to litter decomposition, as this process releases organic acids into the soil. Further research is needed to disentangle inter- from intraannual pH changes, especially with repeated measures within one year. A study by Pham et al. (2018) conducted in Tain Rai mine too, revealed moderately to slightly acidic soil conditions, with an average pH of 6.0–6.8 (H_2O) and 5.5–6.0 (KCl) in the topsoil. Therefore, the pH values observed in the experimental field are notably lower.

The electrical conductivity (EC) of the soils studied is very low – consistently <200 µS cm^{-1} –indicating non-saline conditions and a low concentration of dissolved ions in the soil solution. Unfortunately, EC measurements were not available for 2023, so a complete picture of temporal changes throughout the recultivation process cannot be presented. Between 2021 and 2022, no clear temporal trends in EC were observed. Only two sub-plots showed a slight increase over time, but these changes were not statistically significant, as indicated by overlapping error bars. Notably, sub-plot B exhibited greater variability in EC values. In the absence of high salinity, variations in EC are typically linked to differences in soil texture or water-holding capacity. Since soil texture is uniform across the experimental site, the observed fluctuations in EC are more likely due to inconsistent management practices, such as variable fertilizer application.

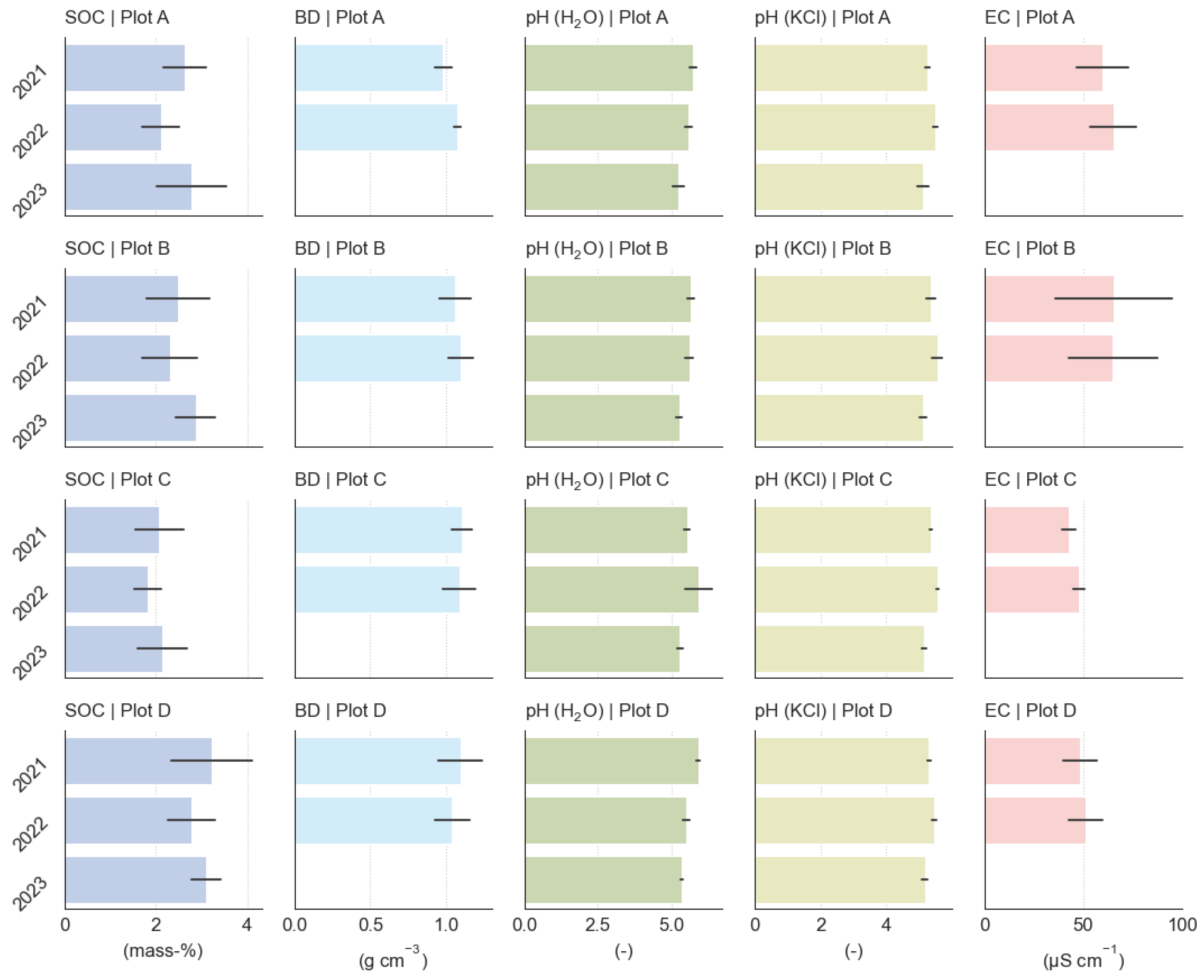

Figure 5: Physical and chemical soil variables by sub-plot and investigation year. Temporal changes are shown by year, except for the variables BD and EC which were discontinued after 2022. Each column corresponds to a specific variable: SOC (soil organic carbon), BD (bulk density), pH (H_2O), pH (KCl), and EC (electrical conductivity). Error bars represent the standard error of the mean (n = 12 for SOC and pH; n = 8 for BD and EC per bar).

3.1.2 Nutrition status

Understanding the nutrient status of soils on the post-mining site is essential in order to evaluate the current soil fertility and guide effective recultivation strategies. This section presents key soil chemical indicators that describe the quality of organic matter, the capacity to retain nutrients, and the availability of essential macronutrients necessary for plant growth. The C/N ratio is a fundamental indicator of soil organic matter quality and microbial activity, reflecting the rate at which organic matter decomposes and the potential for nutrient cycling. Figure 6 presents the C/N ratios for all experimental plots, offering insights into the balance between carbon and nitrogen. Across all plots, the C/N ratio ranges from 23 to 27, indicating moderate values. Plot C exhibits the lowest C/N ratio (23.3 ± 2.8), while Plot D records a slightly higher average ratio (27.3 ± 4.9). These values suggest adequate nitrogen availability relative to carbon, facilitating efficient organic matter decomposition and nutrient release to plants – key indicators of good soil fertility and biological activity at the experimental sites. Temporal analysis reveals consistent

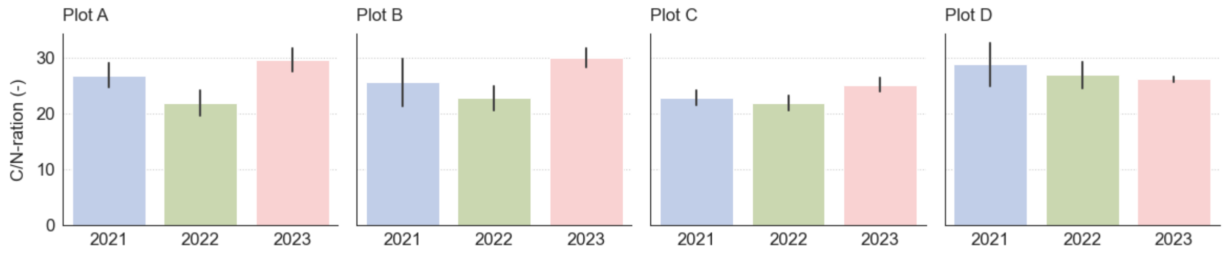

Figure 6: Carbon to Nitrogen ratio (C/N-ratio) constraint by plot. Error bars represent the standard error of the mean (n = 4 per bar).

patterns in Plots A, B, and C, with the lowest C/N ratios observed in 2022 following the first planting cycle and the highest in 2023. This trend aligns with fertiliser application during the initial planting cycle, which increased nitrogen input. Conversely, Plot D displays an inverse pattern, with the widest C/N ratio in 2021 and the narrowest in 2023, though these differences are not statistically significant. The observed temporal dynamics in Plots A, B, and C are consistent with expected responses to fertiliser application. The atypical behaviour in Plot D may be attributed to grazing activities, as the plot borders the VA06 area, which is commonly used for animal feedstock. Regular observations of cattle traces (dung and footprints) suggest that livestock may have favoured Plot D for resting due to its proximity to VA06. Supporting this hypothesis, He et al. (2011) demonstrated a reduction in C/N ratio with increasing grazing intensity. Alternatively, inconsistent fertiliser application across the experimental field could also explain the deviating behaviour in Plot D.

Within the soil, Clay particles and organic matter (SOM) have a net negative charge at their surfaces. Due to these surface charges, soils can reversibly fix cations that are relevant for plant nutrition, such as calcium, magnesium, potassium, and sodium. The total number of cations that a soil can hold is expressed as its cation exchange capacity (CEC), which describes a soil's ability to bind and store cationic nutrients. As the proportions of clay and SOM vary between soils, so does their CEC. Figure 7 presents the effective cation exchange capacity (CEC_{eff}), measured at the soil's actual pH. Because CEC declines at lower pH levels, CEC_{eff} reflects the soil's cation-binding capacity under natural conditions. On average, CEC_{eff} values for the plots range from 4.69 ± 0.75 (Plot B) to 5.41 ± 0.94 (Plot A). Over time, CEC_{eff} shows a slight decrease in Plots C and D, while remaining stable in Plots A and B. This trend likely mirrors the dynamics of soil organic carbon (SOC), given the well-established relationship between SOM and CEC_{eff}. When compared to reference values for silt loam soils – typically 15-25 meq 100 g^{-1} – the CEC_{eff} of the Lam Dong pilot site falls below this range, aligning instead with values characteristic of coarser-textured soils. Consequently, the CEC_{eff} at this site is rated as low to moderate, indicating soils of limited fertility. The reduced cation exchange capacity is probably attributable to low SOC content, limited clay fractions, and a moderately to strongly acidic soil pH.

When compared to reference values for silt loam soils – typically 15-25 meq 100 g^{-1} – the CEC_{eff} of the Lam Dong pilot site falls below this range, aligning instead with values characteristic of coarser-textured soils. Consequently, the CEC_{eff} at this site is rated as low to moderate, indicating soils of limited fertility. The reduced cation exchange capacity is probably attributable to low SOC content, limited clay fractions, and a moderately to strongly acidic soil pH.

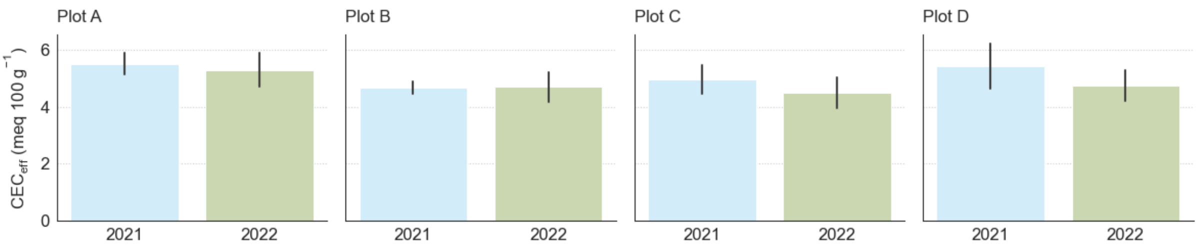

Figure 7: Effective soil cation exchange capacity (CEC_{eff}) constraint by plot. The unit of CEC_{eff} is milliequivalents per 100 grams of soil (meq 100 g^{-1}) as a measure concentration per unit of volume as different cations hold differing positive charges. Error bars represent the standard error of the mean (n = 4 per plot and measurement campaign).

The availability of the three main macronutrients – nitrogen (N), phosphorus (P), and potassium (K) – directly impacts plant growth and ecosystem recovery. Figure 8 illustrates the plant-available concentrations of these nutrients across the four plots. Overall, phytoavailable macronutrient levels are comparable among plots, except for Plot C, which exhibits slightly lower values for all three nutrients. Temporal trends reveal distinct patterns: plant-available nitrogen drastically dropped from 730.3 ± 132.2 mg kg^{-1} in 2021 to 25.3 ± 17.8 mg kg^{-1} in 2023. This sharp decline likely results from fertiliser application only at the start of the first cultivation cycle in 2021. In contrast, plant-available phosphorus showed a modest increase from 2.0 ± 0.7 mg kg^{-1} in 2021 to 2.7 ± 1.2 mg kg^{-1} in 2023, while potassium slightly decreased from 20.5 ± 3.4 mg kg^{-1} to 18.8 ± 2.7 mg kg^{-1} over the same period. These trends suggest the onset of soil microbial activity decomposing organic matter, gradually releasing phosphorus and potassium. When compared to reference values for Ferralsols, plant-available nitrogen aligns with typical ranges (5-20 mg kg^{-1}) by the end of the monitoring period. However, phosphorus and potassium concentrations fall below typical values (5-15 mg kg^{-1} for P and 30-150 mg kg^{-1} for K). This discrepancy is likely due to the high fixation capacity of iron and aluminium oxides in Ferralsols, which immobilises these nutrients. While managed soils can achieve slightly higher concentrations, the observed levels reflect the inherent nutrient dynamics of these soils.

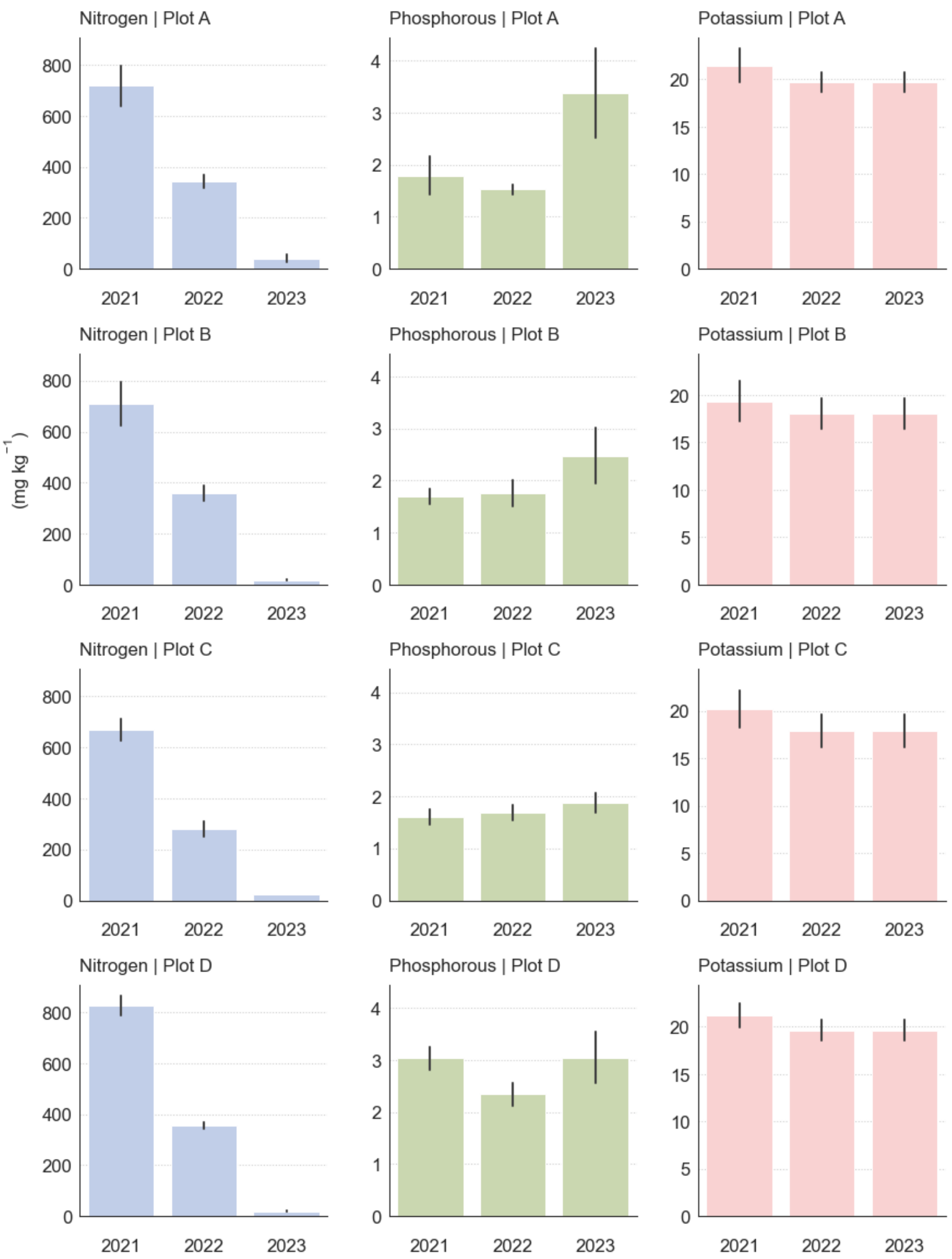

Figure 8: Temporal development of the major plant nutrients expressed as phytoavailable nitrogen ($NH4^+$-N = ammonium nitrate), phosphorus (P_2O_5 = phosphorus pentoxide) and potassium (K_2O = potassium oxide) at 0-30 cm soil depth, stratified by plot. Data bars represent means (n = 4 per variable, plot, and sampling campaign), with error bars indicating the standard error of the mean.

3.1.3 Trace metal contents and temporal dynamics

The origin of trace metals in soils are both, natural processes and anthropogenic. The dominating natural source of trace metals is for example their release from parent material during pedogenetic process.

Volcanic activity and forest fires can also release trace metals in the environment which then enter as atmospheric deposition the soil system. However, the main reason of elevated and potentially harmful trace metal concentrations in soils are human activities such as industrial activities, agricultural practices and urban pollution (Angon, et al., 2024). As trace metals are of persistent nature, it is of paramount importance to mitigate the spread of trace metals in environmental systems to avoid human exposure and safeguard human and environmental health. Figure 9 displays the measured trace metal contents in the soils of the Lam Dong experimental site. To better align the metal contents, the maximum permissible limit for each trace metal for agricultural land use according to Vietnamese legislation (QCVN 03:2023/BTNMT, 2023) is plotted as solid horizontal line. With the exception of chromium, all levels of metal contents fall clearly below the maximum permissible limit. At this point it is important to note that toxicity is highly metal-specific. Out of the eight trace metals considered here, the Swedish Environmental Protection Agency rates zinc as moderately hazardous; chromium (without Cr IV), copper and nickel as very hazardous; as well as arsenic cadmium, chromium (Cd IV), mercury and lead as extremely hazardous (Swedish Environmental Protection Agency, 2002). Considering this rating, only the elevated chromium levels are of major concern as all the other extremely hazardous metals are clearly below the limit for agriculture. To closer align the chromium levels, the limit values for forestry (dashed line) and mining (dotted line) are plotted additionally for this element in Figure 9. Across all plots, average arsenic concentrations slightly exceed the regulatory limit for mining activities. Since bauxite extraction is confined to the upper 5-10 m of soil, contamination by chromium from mining residues is considered unlikely. Ferralsols, characterised by their acidic nature, low organic matter content, and high concentrations of iron and aluminium oxides, significantly influence chromium speciation and retention. These soil properties likely account for the observed chromium levels, which are more closely associated with the geochemical composition of the parent material than with mining activities.

In comparison between the planting systems, no clear patterns can be observed as average metal contents are very similar between the plots (Figure 9). Only arsenic levels are significantly higher at the VA06 plot compared to the Acacia plot. Also, the temporal development shows no clear trend in metal contents as the deviation between different sampling campaigns is generally low without distinct patterns such as an increase or decrease with time. More likely, the deviation in metal levels in the soil between single campaigns or planting systems reflects the general heterogeneity of trace metal patterns as always composite samples were analysed, always from the same sub-plot (see Section 2.2, Page 4) but never from exactly the same points.

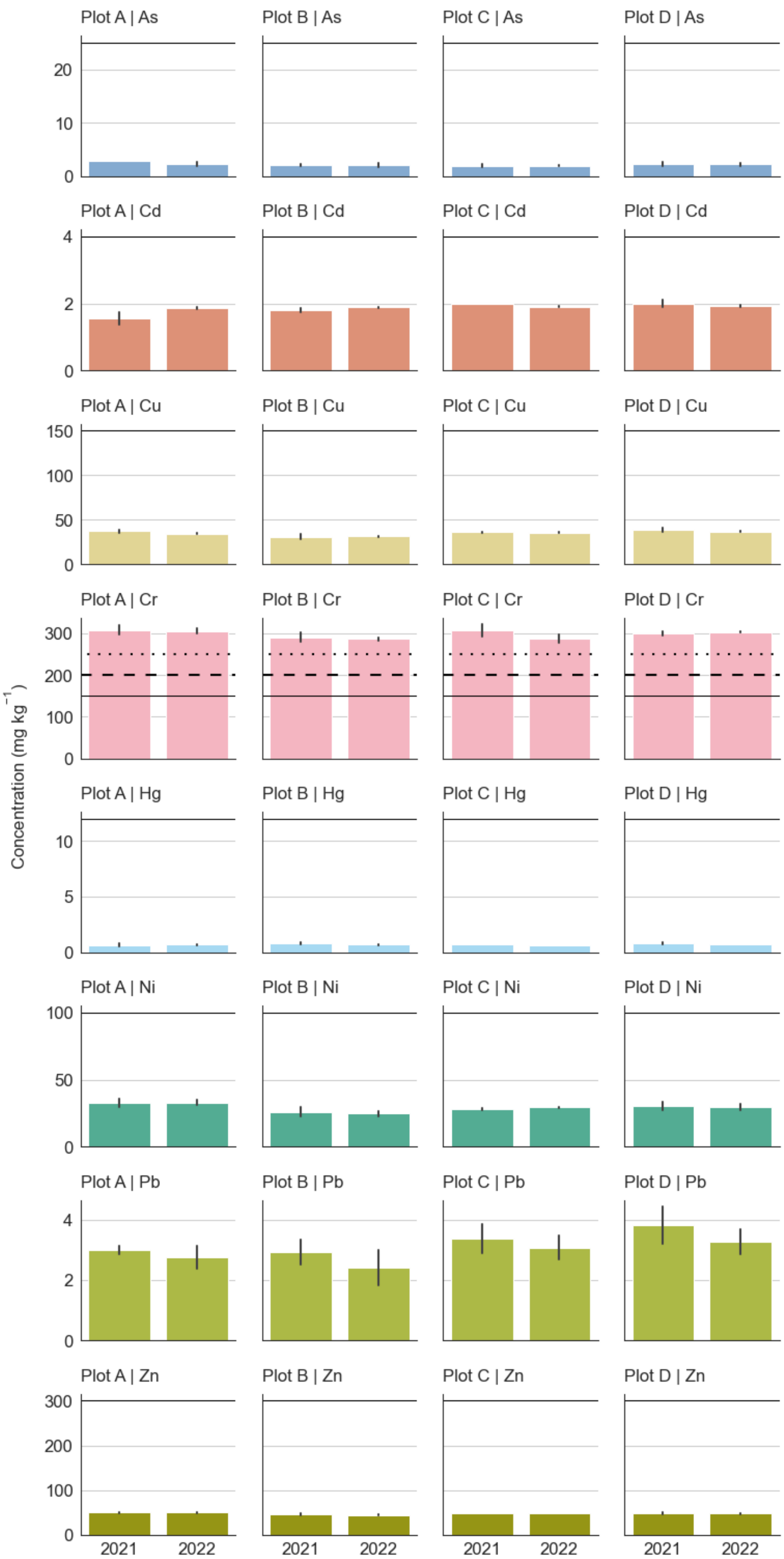

Figure 9: Trace metal contents (mg kg^{-1} soil) by planting system and sampling campaign. The left, middle, and right columns display data for the VA06, Acacia, and crop rotation plots, respectively. Each row corresponds to a different trace metal, as indicated by the color-coding. As the second sampling campaign was conducted in different years for the different planting systems, the years differ between rows (year 2024 for the VA06 plot and year 2022 for the acacia plot). Solid lines denote the maximum permissible limits for each trace metal under Type 1 land use (QCVN 03:2023/BTNMT, 2023), with additional dashed and dotted lines showing Type 2 and Type 3 limits for chromium. Data bars represent means (n = 5 per variable, plot, and sampling campaign), with error bars indicating the standard error of the respective land use categories: Type 1 (feed/food production, residential), Type 2 (forests, public buildings, energy/telecom infrastructure), and Type 3 (industry, mining, transportation). Error bars represent the standard error of the mean (n = 5 per variable, plot, and campaign).

3.1.4 Soil hydrology

The measured soil water retention and the fitted retention curve is illustrated in Figure 10. Generally, the curve expresses the relationship between the soil water content (theta) and the soil water potential (pF) also called matric potential. The relation between both values characterises the soil water household and illustrates how much water a soil holds at different tensions (moisture states). More precisely spoken, the shape of the curve reflects the soil's ability to retain and release water as moisture conditions change. As such the soil water retention curve is essential to predict soil water storage, soil seepage water, and to assess the plant water availability. The curve characteristics are determined by soil texture in combination with further soil structure affecting parameters like soil biological activity and SOC content. In saturated conditions, around 40% of a given soil volume are water in both layers (ϴ of 0.4, Figure 10). Both layers show a steep decrease for lower pressures (pF <1.8), where the course soil pores and gravimetrically driven soil water movement dominates. Especially in the lower layer the steep decrease in soil water retention between a pF of 2 and 3.5 implies a relatively uniform pore size distribution, where many medium pores empty over a narrow suction interval. The grey shaded area in Figure 10 marks the plant available fraction of soil moisture. It is the part of the retention curve between field capacity at pF 1.8 and permanent wilting point (pF >4.2). Water above the field capacity drains too quickly to be available to plants. Vice Versa, soil water below the wilting point is held too tightly by the soil for plant roots to extract. Whereas the upper layer shows retention properties typical for Silt Loam with a smooth transition from plant-available (pF 1.8) to plant-unavailable water (pF 4.2), the pronounced drop in the lower layer in this range is rather untypical as is suggests a very homogenous pore size distribution. However, both layers have a good moisture storage capacity, as the difference in soil moisture between the pF of 1.8 and 4.2 is around 0.2. As such, 20% of a given soil volume for the lower layer are available for plants – but in the lower layer with a sudden transition from well-watered to dry. In a short review, it was not possible to identify, reference studies assessing the soil water retention characteristics of soils in central Vietnam. Hence, it is difficult to judge if the sharp transition from wet to dry in the lower layer is a typical phenomenon of Lam Dong province. It might be a result of the still developing soil structure, which typically needs decades to recover after disturbance (Baumgartl, et al., 2023). As such the current pore size distribution in the lower layer probably relates to texture-related pores and no secondary ones from soil biological activity.

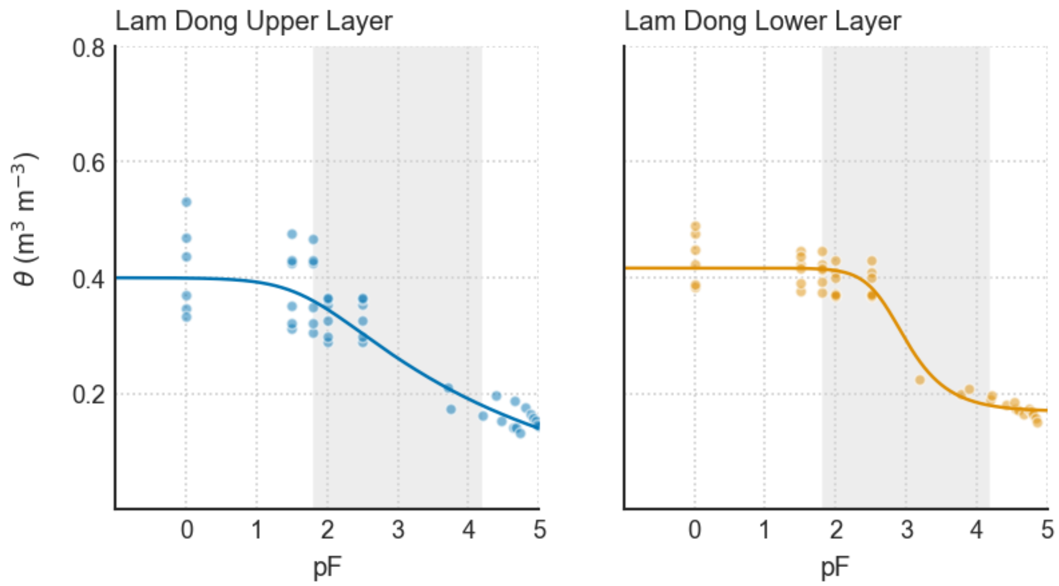

Figure 10: Soil water retention curves fitted to the lab-determined suction heads and given soil water contents. The grey shaded area marks the plant available water (between field capacity and permanent wilting point). Upper layer corresponds to depths of 0-35 cm depth and lower layer to depths of 35-60 cm. The grey shaded area is the range between field capacity (pF of 1.8, from where soils can retain water against gravity) and permanent wilting point (pF of 4.2, from where plants cannot take up any more water as the suction forces are too strong). This grey shaded range expresses the plant available soil moisture for the soils of the experimental field.

The saturated water conductivity was measured using the same experimental design as for the soil water retention characteristics (2 soil profiles on the experimental field and two depths 0-35 cm and 35-60 cm). Similar to the soil water retention the upper two lower layer reveal similar soil hydrological conditions (Figure 11). There is nearly no difference in hydraulic conductivity with 50.0 cm h^{-1} in both layers on average. Both K_{sat} values show a large scatter expressed by the high standard deviation in general. The scatter probably relates to the soil heterogeneity induced by mining and re-deposition of the soil. As already elaborated in the section on the soil water retention curve, soil structure was massively disturbed by mining. In conclusion, the three repetitions for each plot and depths to analyse the K_{sat} are probably too low to capture these large heterogeneity of soil structural properties on the experimental field. Reference values for K_{sat} based on a global database with large sample sizes report typical ranges of K_{sat} for the textural classes investigated here between near zero up to 53.9 cm h^{-1} (García-Gutiérrez, et al., 2018). Median values are typically around 5.2 cm h^{-1} which clearly deviates from both soil layer. However, as already stated before, SOC and soil biological activity influence soil structure too. Influence of these parameters decreases with increasing depth and might be the reason that soil texture not mirrors typical K_{sat} in the investigated layers. Further investigations with higher repetitions are required to clearly differentiate the effect of soil biological activity and SOC here and to exclude errors either induced by sampling or lab-analysis or both.

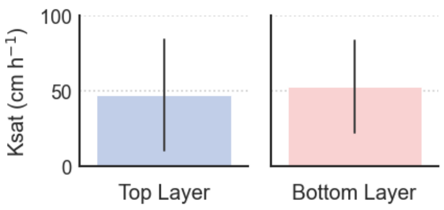

Figure 11: Saturated water conductivity (K_{sat}) of undisturbed soil cores sampled in 2023 in two soil profiles of the Lam Dong experimental site. Top Layer corresponds to sample from 0-30 cm depth and Bottom Layer to samples from 30-60 cm depth. Error bars represent the standard error of the mean (n = 6 per depth).

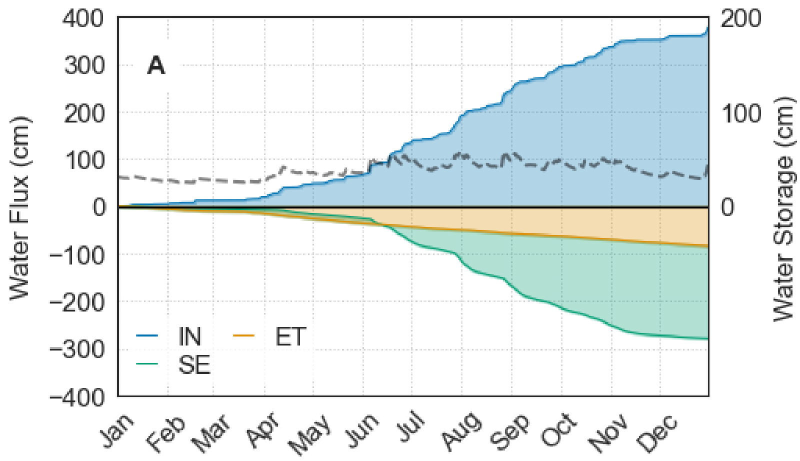

Figure 12: Simulated annual water balances of the year 2023. Positive values indicate fluxes into the soil profile and vice versa for negative values. "IN" and "ET" denote the infiltration and evaporation at the upper boundary and, "SE" fluxes through the lower boundary (deep seepage). The dashed line illustrates the total water volume in the soil profile (storage).

To understand how water moves through the soils at the experimental site, the soil water balance was calculated for the year 2023 based on soil hydrological properties and meteorological boundary conditions. This balance provides important information on the partitioning of incoming precipitation into evapotranspiration, groundwater recharge, and soil water storage. These insights are crucial for assessing both water availability for plants and the movement of dissolved substances through the soil. As shown in Figure 12, the simulated soil water balance revealed an annual infiltration of 3,654 mm. Of this, 845 mm (23%) was lost to evapotranspiration, while 2,809 mm (77%) exited the profile as deep seepage. A distinct dry season was observed from November to April, characterized by minimal infiltration and seepage. Although direct validation was not possible, the simulated evapotranspiration values fell within ranges reported for the region (Ha, et al., 2023; Sayyadi, et al., 2025; Tran, et al., 2023), lending confidence to the model.

3.1.5 Carbon Quality

Next to the question of total soil organic carbon (SOC) the soil carbon dynamics are of interest to better understand the impact of land use, biological activity and carbon sequestration in soils. Generally, the SOC can be divided into the labile pool and stable pool based on its stability and turnover time. Whereas carbon in the stabile SOC pool is chemically or physically protected with long turnover time (250-5,000 years), carbon in the labile SOC pool is readily decomposable and responsive to management and environmental changes. The turnover rate in this pool is much faster and plays a functional role in nutrient cycling and soil fertility due to its decomposition and release of nutrients. Literature values on typical turnover rates within this pool range from 20-100 days (Zou, et al., 2005) up to 3 years (Sanderman, et al., 2017). As such, the labile fraction is of major interests in questions of soil carbon quality and considered more closely here. Figure 13 shows three soil organic fractions from two soil profiles of the experimental field all belonging to the pool of labile soil organic carbon and the subgroup of active carbon within this group. The cold-water soluble carbon fraction (CWSC) has lowest values in both investigated soil depths and represents the most readily available and mobile organic carbon in soils.

Figure 13: Different soil carbon fractions determined at the experimental site. CWSC is the cold-water soluble carbon, HWSC is the hot water-soluble carbon and POXC the permanganate oxidisable carbon. Upper layer corresponds to 0-30 m depth and lower layer to 30-50 cm depth. Sampling was done in April 2024 (n = 6 per variable and depth). Error bars represent the standard error of the mean.

CWSC is especially an indicator of short-term changes in soil management or environmental conditions. Highest values in the labile carbon pools were measured for the permanganate oxidizable carbon (POXC) which is more stable than hot and cold-water soluble carbon but still turns over within months to years. POXC is widely used as a sensitive indicator of soil quality and management impacts. In between are contents of the hot water-soluble carbon fraction (HWSC) which is slightly less labile than CWSC but still represents a readily decomposable carbon pool. HWSC and POXC both correlate strongly with microbial biomass and soil fertility and are useful for assessing soil health and the immediate availability of carbon for microbial activity (Culman, et al., 2012; Hurisso, et al., 2016). This fact is probably the reason of the significantly higher HWSC and POXC contents in the upper layer compared to lower layer as microbial activity and biomass input normally reduces with increasing depth.

To better rate soil quality based on the labile carbon fractions, Table 4 shows the share of total soil organic carbon of the three labile carbon fractions. CWSC fractions are typically very small in soils, making up less than 1% of total SOC. The same is true for the soil at the experimental field. HWSC share of total SOC is slightly higher but still within typical values in soils (<1%). POXC concentrations, ranging from 2.1-2.6%, fall within the typical share of total SOC (1-5% of total SOC), too. As the latter fraction is mainly used as indicator for soil quality, the overlap with typical shares on total SOC gives strong evidence for a soil quality at the experimental field at least as good as average. The total share of the considered labile pool (CWSC, HWSC, and POXC) ranges from 3.2-3.9% of total SOC. As these three fractions all belong to the active and thus easily decomposable fraction, this low share is a good results in questions of climate change mitigation. Because vice versa, this low share implies a strong bias of typical share of total SOC towards the stable carbon pool and thus long-term carbon sequestration in the soil.

Table 4: Share of labile carbon on total soil organic carbon. CWSC is the cold-water soluble carbon, HWSC is the hot water-soluble carbon and POXC the permanganate oxidizable carbon. Upper layer corresponds to 0-35 m depth and lower layer to 35-60 cm depth. Sampling was done in April 2024.

Sample	Fraction CWSC	Fraction HWSC	Fraction POXC	Σ
	(%)	(%)	(%)	(%)
Upper Layer	0.24	0.88	2.75	3.87
Lower Layer	0.20	0.84	2.14	3.18

3.1.6 Soil Erosion

Soil erosion modelling result are presented for two land-use scenarios (Figure 14). The “Cassava Cultivation” scenario (upper row) represents land use under cultivated crops, while the “Bare Soil” scenario (lower row) simulates water-induced soil erosion without protective soil cover. The “Sediment Local” layer quantifies site-specific sediment erosion yields at the raster cell level (20 × 20 cm), reflecting local soil erodibility. The “Sediment Accumulation” layer illustrates cumulative sediment deposition downstream within the watershed, aggregating local yields to depict basin-wide accumulation patterns. Under cassava cultivation, erosion patterns are minimal, with light colors dominating the map and indicating very low erosion values. The maximum erosion rate in this scenario is 3.2 kg year^{-1} pixel^{-1} (80 kg year^{-1} m^{-2}), confined to isolated hotspots along the southern border of the experimental site. The site-wide average erosion rate is 0.19 kg year^{-1} pixel^{-1} (4.75 kg year^{-1} m^{-2}). Sediment accumulation at the southern outlet totals 73 Mg year^{-1}, equivalent to the total soil loss by water erosion in this scenario.

In contrast, the bare soil scenario reveals substantially higher erosion rates, with dark brown spots distributed across the site and sediment accumulation clearly following overland flow patterns, forming a branching network converging at the southern outlet. Average erosion in this scenario reaches 0.93 kg year^{-1}pixel^{-1} (23.25 kg year^{-1} m^{-2}), with peak values of 15.88 kg year^{-1}pixel^{-1} (397 kg year^{-1} m^{-2}). Sediment accumulation at the southern outlet is 36.29 Mg year^{-1}, underscoring the severe soil loss under bare conditions. These findings highlight the effectiveness of cassava cultivation as a mitigation strategy against water erosion in high-rainfall environments, even on nearly flat terrain (elevation range: 882–887 m a.s.l.).

The bare soil scenario mirrors traditional recultivation practices on neighboring mine sites, where acacia and pine are planted in rows without ground cover. The results emphasize the critical need for early establishment of soil cover during recultivation to prevent serious soil degradation by water erosion, regardless of terrain slope. These findings align with Singh et al. (2023), who found bare post-mining plots eroded at up to 583 Mg ha^{-1} year^{-1} using RUSLE, versus near-zero rates under revegetation. It partially disagrees with Chuenchum et al. (2020) in Thailand, where cassava itself accelerated erosion on steeper slopes, underscoring site-specific topography. Northern Vietnam studies by Trinh (2007) report cassava plots losing 1,360 kg ha^{-1} over events versus 45 kg ha^{-1} in terraced watersheds.

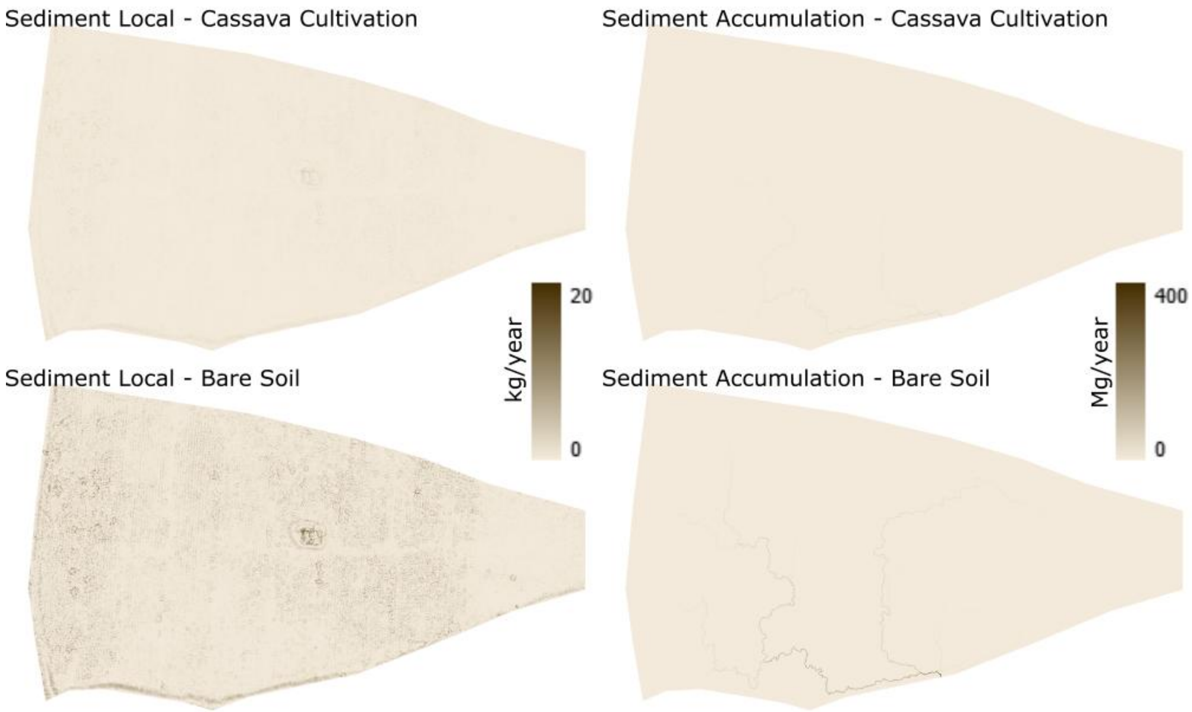

Figure 14: Simulated annual soil erosion by water for two land-use scenarios – cassava cultivation (top row) and bare soil (bottom row). "Sediment Local" (left column) indicating soil loss per pixel in kg year^{-1} and "Sediment Accumulation" (right column) showing the total eroded soil reaching each pixel from upstream in Mg year^{-1} (Megagram). The pixel resolution is 20 x 20 cm in each sub-figure.

3.2 Cassava (*Manihot esculenta*)

3.2.1 Planting Cycle 2021-2022

To determine the yield of cassava tubers, 10 individual plants were sampled per sub-plot during the harvest in 2022 and weighted directly on the experimental site. The mean cassava root yield across all plots was 8.42 ± 4.38 t ha^{-1} (Figure 15). However, plots 6, 8, 10, and 12 (cf. Figure 14, Page 4) – where parts of the experimental site experienced almost complete crop failure – significantly influenced this average. Accordingly, the tuber yields range from 6.97 ± 4.48 t ha^{-1} (Plot C) up to 9.89 ± 4.28 t ha^{-1}. Compared to the average cassava root yield of 12.67 and 20.86 t ha^{-1} reported for the Central Highlands and for complete Vietnam (Le, et al., 2019), the yields of the experimental site represent approximately 66% and 40% of the regional and national benchmarks, respectively. These results highlight the site's potential for cassava cultivation. Notably, plots 15 and 7 achieved mean yields of 11.57 t ha^{-1} and 11.38 t ha^{-1}, respectively. Extrapolated maximum yields from individual plants reached as high as 22.1 t ha^{-1} (plot 11) and 20.8 t ha^{-1} (plot 15), exceeding the regional average clearly.

Nonetheless, yields fell short of expectations primarily due to challenges encountered during the preparation and early growth phases, exacerbated by COVID-19 restrictions. Key factors included insufficient water supply in the first two months, as the irrigation system was not completed in time, and delayed application of organic fertilisers, which led to excessive branching and flowering at heights of 50-70 cm. Additionally, theft of about 30% of the highest-yielding plants further reduced overall yield.

The observed mean stem height of 67.08 ± 11.77 cm is notably lower than that typically recorded in conventional cassava cultivation areas (Figure 15). Given the exposed, flat terrain and absence of windbreaks, this reduced height likely represents a physiological adaptation to strong winds, minimising the risk of stem breakage.

Figure 15 (bottom row) presents key properties of cassava tubers measured in the lab. On average, the tubers contain a high starch concentration of 72.03 ± 8.18% and a low fibre content of 1.51 ± 0.32% (both values based on dry matter). These figures suggest the tubers were harvested at an ideal stage: the starch content is at the upper end of typical values reported in the literature (Silva, et al., 2023), while the fibre content is relatively low – well below the usual range of 2-6% of dry mass. Together, these properties indicate that the tubers are mature enough for efficient starch conversion but not overmature, which would lead to higher fibre levels and potentially reduce processing efficiency. This balance makes them particularly well-suited for ethanol production, offering both high substrate availability and ease of processing. When comparing the different plots, no clear spatial patterns emerge. Starch content is highest in Plot C (79.05 ± 2.07%), while fibre levels are elevated in Plots B and C (1.87 ± 0.04% and 1.61 ± 0.36%, respectively). The higher fibre content in these plots may reflect greater tuber maturity, which could explain the increased starch concentration in Plot C. However, Plot C also produced the lowest yield, suggesting that less favourable growing conditions might have contributed to the higher starch levels. With only one planting cycle's data, it is not possible to draw definitive conclusions about these variations. Additional planting cycles and replicates will be necessary to disentangle separate natural variability from environmental effects.

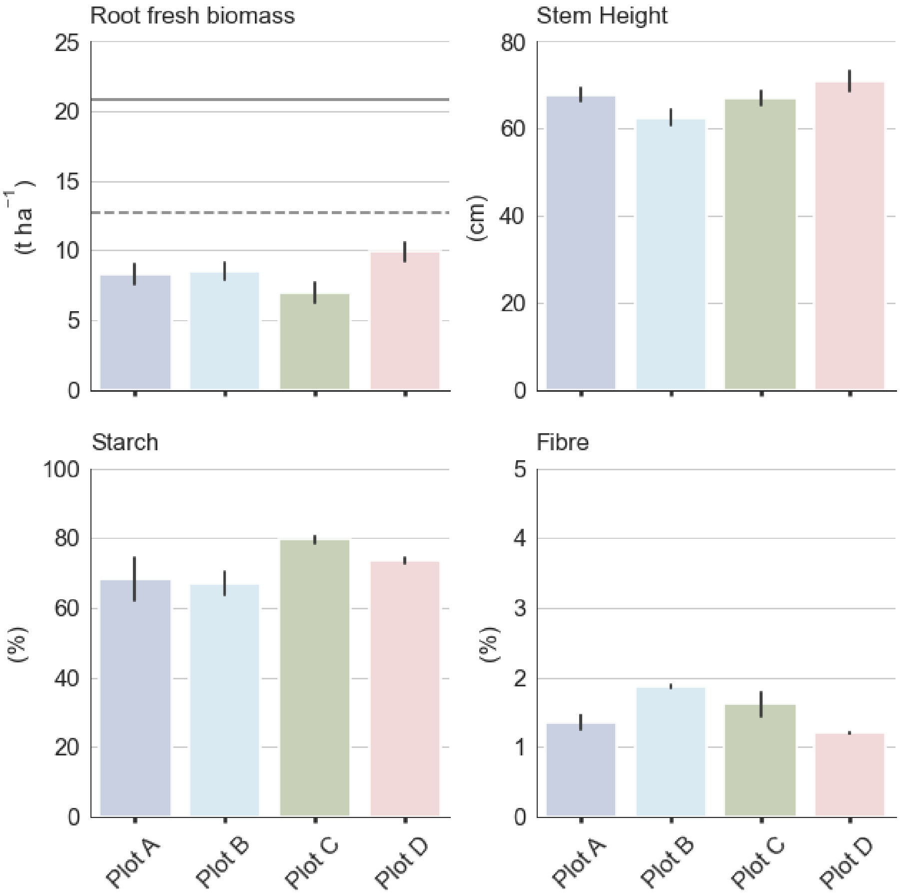

Figure 15: Field-measured fresh cassava root yield (left) and stem height (right) at harvest in 2022 (top row), and lab-determined starch and fibre concentrations (dry weight basis, left and right, respectively; bottom row). Bars show the mean per subsample with error bars indicating the standard error of the mean (n = 40 for yield and height per bar; n = 4 for starch and fibre per bar).

3.2.2 Planting Cycle 2023-2024

In April 2023, a second rotational planting of cassava was conducted at the experimental site in Lam Dong using cuttings from the same seed supplier as the successful 2021 planting. One month after planting, initial signs of cassava mosaic disease virus (CMD) appeared (Figure 16 and Figure 17). While CMD is typically managed by removing and replanting infected plants – as successfully done in 2021 – symptoms rapidly spread to nearly 100% of the plants within a week. This unprecedented infestation suggested that the mother plants used for the cuttings were already infected with CMD, a virus known to cause stunted leaf growth, reduced plant vigor, and significant yield loss in root tubers. Although CMD has been documented in Africa and India, its presence in Vietnam was first confirmed in 2016, with limited reports of widespread infection (Hareesh, et al., 2023; Hoang, et al., 2024). Given the manageable outbreak in 2021 and no new evidence of increased CMD prevalence, no additional preventive measures were implemented prior to the 2023 planting. However, due to the severe impact on root development and the extensive infection, it was decided to destroy the entire April 2023 planting.

To mitigate the risk of persistent soil-borne virus, a virus-resistant cassava variety (HN1)—recently approved for agricultural use in Vietnam at the end of 2022—was selected for a new planting in early June 2023. Initially, the new plantation showed no signs of mosaic disease, indicating a successful establishment.

However, the 2023 summer monsoon in Lam Dong Province was exceptionally severe (Figure 18), leading to repeated flooding and waterlogging at the experimental site in Bao Lam (Figure 20). As a result, approximately 60% of the June-planted cuttings rotted, while another 35% germinated but exhibited no root growth and were expected to die (Figure 19 and Figure 21). Only about 5% of the plants demonstrated normal development. Given the poor prognosis, the second planting in 2023 was also terminated.

Figure 16: Germination of cassava and mung beans in May 2023.

Figure 17: First signs of mosaic virus disease after one month of planting, as indicated by leaf distortion and stunted growth.

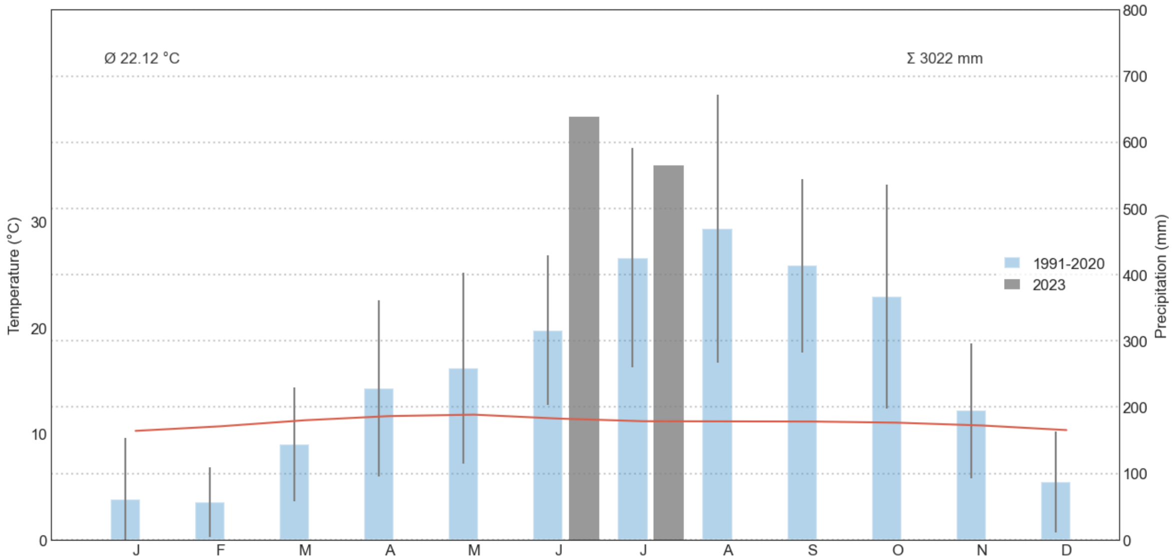

Figure 18: Climate graph for the Bao Loc meteorological station. The blue bars show the long-term average (30 years) of monthly cumulative precipitation. The standard deviation is indicated by the line at the top of each bar to show the inter-annual variability of monthly precipitation. The grey bars show the cumulative precipitation for June and July 2023. The figure clearly shows that June precipitation is above its long-term average.

Despite the absence of a successful harvest, the 2023 trials provided critical insights:

- The arrival and spread of cassava mosaic disease virus in Vietnam must now be considered in agricultural planning.
- The early and intense monsoon season underscores the increasing impact of climate change, highlighting the need for recultivation approaches that prioritise soil protection and agroecological resilience to extreme weather events.

Figure 19: Mother plants of virus-resistent variety HN1 used for replanting in June 2023.

Figure 20: Flooded parts of the Lam Dong experimental site after an exceptionally heavy monsoon in June 2023.

Figure 21: Abnormal cassava growth due to rotten cuttings after partial flooding.

3.2.3 Ethanol Capacity

The hydrolysis efficiency of dried cassava was superior to that of fresh cassava, as evidenced by higher reduced sugar yields (Table 5). During fermentation, reduced sugar concentration decreased rapidly within the first 24 hours, then gradually from 24 to 72 hours, reaching 0.9 g L^{-1} at the end of the process. This indicates near-complete nutrient utilisation by 72 hours. From 4 L of fermentation broth, 685.6 mL of 60.5° ethanol was obtained, equivalent to 327.2 g of ethanol. The theoretical ethanol yield from 2 kg of fresh cassava (starch content: 84.2%, dry matter: 38.4±0.2%) was calculated as 367.1 g. The fermentation efficiency was 89.2%, exceeding the 85.4% reported by Wangpor et al. (2017). This improvement is attributed to the removal of toxic components during drying, higher sugar concentration in the fermentation medium, and the use of a more efficient *S. cerevisiae* strain.

Table 5: Reduced sugar after hydrolysis of 2 kg of fresh cassava tuber in the laboratory.

Sample	Reduced Sugar	Brix
	(g L^{-1})	(°Bx)
Dried cassava	87.4	21.3
Fresh cassava	72.8	21.2

3.2.4 Carbon Storage

A key objective of the project is to assess the impact of soil conservation on climate change mitigation, alongside the provision of renewable energy. To evaluate this, soil organic carbon (SOC) content was measured annually at the experimental site. Soil samples were collected before planting and after harvest each year, with 150 individual sampling points distributed representatively across the site per campaign.

Table 6 presents the annual average SOC contents and calculated stocks for the upper 30 cm of soil at the experimental site. While a slight decrease in SOC was observed in 2022, the overall trend since the initiation of recultivation with energy crops indicates stabilisation of SOC levels, with a gradual increase over time. The temporary decline in 2022 is likely attributable to a peak in SOC mineralisation by heterotrophic soil organisms, as the natural soil carbon cycle adjusted to the new conditions. Initially, mineralisation rates exceeded carbon inputs, but this imbalance appears to have stabilised as the system matured. Combining SOC data with known soil physical characteristics allows for the calculation of carbon stocks. After three years of recultivation, the average carbon stock at the test site is estimated at 87.6 t ha^{-1}, or 140.16 t SOC across the entire site. These results highlight the significant potential of optimised recultivation approaches to enhance soil protection and contribute to climate change mitigation.

Table 6: Soil organic carbon (SOC) stocks (0-30 cm depth) at the experimental site (1.6 ha) by measurement year, with bulk density held constant due to insufficient replicates for temporal analysis. Total SOC stocks are aggregated across the entire site; total CO_2eq is calculated as SOC × 3.67. Sample size: n = 16 per campaign.

Year	SOC	BD	SOC stock	Total SOC	Total CO_{2eq}
(-)	(%)	(g cm^{-3})	(t ha^{-1})	(t)	(t)
2021	2.60	1.07	83.46	306.30	490.08
2022	2.25	1.07	72.23	265.07	424.11
2023	2.72	1.07	87.31	320.44	512.70

3.2.5 Trace Metal Content and Soil-Plant Transfer Pathway

As trace metals are persistent pollutants, it is important to prevent a spreading these elements in our environmental system. For this reason, the trace metal content was determined in the harvested cassava plants. Figure 22 displays both, the trace metal content in soil and biomass to identify a possible trace metal transfer along the soil-plant pathway. For simplicity, only the trace metals rated as extremely hazardous (see Section 3.1.3, Page 21) are considered here. Additionally, iron, zinc, manganese, copper, molybdenum and nickel are essential micronutrients for the healthy growth and development of cassava (Roberto Baizi e Silva, 2025). Consequently, plants actively force uptake of these metals. Considering the extremely hazardous trace metals here, arsenic transfer is not verifiable, and cadmium transfer is negligible (Figure 22). Similarly to cadmium, chromium uptake by the cassava plants is also negligible small. At first glance, mercury uptake appears to be extremely high in the stem/tuber fraction. However, this is most likely an error due to sample contamination or measuring error, as the mercury content in the plants is higher than in the soil. Only lead shows higher transfer rates from the soil into the plant, with values in the stem fraction being approximately half of the soil content (right column, Figure 22). Oriji et al. (2021) examined trace metal uptake by staple food crops on farmland near mining sites and found bioaccumulated toxic levels in cassava tubers especially for Pb out of the elements considered here. As lead preferentially accumulates in the stem and not in the tuber, there is currently no risk for ethanol production or dietary use. However, the stems should stay on site to prevent any environmental dispersion of lead.

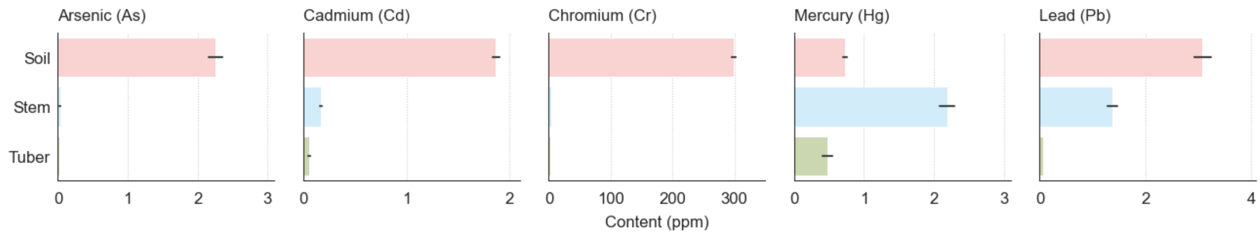

Figure 22: Comparison of trace metal contents in the soil and the different fractions of biomass to estimate the metal uptake rate by the cassava plants. For the sake of simplicity, metal relocation is only considered here for the trace metals rated as extremely hazardous (see Section 3.1.3, Page 21). The bars represent the mean for each subsample. The black line shows the standard error from the mean. The sample size is n = 32 per element and fraction.

4 Discussions

4.1 Recultivation Status and Climate Change Mitigation

Effective soil recultivation not only restores degraded post-mining landscapes but also plays a critical role in climate change mitigation by enhancing soil carbon sequestration and improving ecosystem functions.

4.1.1 Soil Quality and Fertility

Soil pH has slightly decreased, reaching the strongly acidic range typical of Ferralsols. Continued monitoring is essential, as further acidification could inhibit plant growth. However, the observed partly decrease in soil bulk density and slight increase in soil organic carbon (SOC) are positive indicators of improved soil quality. These changes reflect key recultivation processes: soil structure reformation, enhanced microbial biomass and activity, and vegetation restoration.

Among the different plots, especially the C/N ratio is the only systematically deviating physicochemical parameter in spatial comparison. Contrary to the plots A-C, here C/N decreased by time as N contents drastically dropped. This is likely because of maintenance irregularities such as less topsoil replaced here after mining or less fertiliser application compared to the remaining site. All other physicochemical soil parameters reflect spatially heterogeneous physicochemical soil conditions most likely tracing back to the severe soil disturbance during mining. However, BD and SOC equal averages for Ferralsols in Vietnam which is an interesting finding as it suggests that mining disturbances not overprinted the characteristics of the native soil type.

In terms of soil fertility, the pilot site demonstrates low to moderate fertility, primarily constrained by effective cation exchange capacity (CEC_{eff}) values averaging 4.69–5.41 meq 100 g^{-1} across plots. These levels fall well below the 15–25 meq 100 g^{-1} typical for silt loams, aligning instead with coarser-textured soils due to low soil organic carbon (SOC), limited clay content, and moderately to strongly acidic pH. Plant-available macronutrients reveal comparable levels across plots, except for slightly lower concentrations in Plot C. Nitrogen plummeted from 730 mg kg^{-1} in 2021 to 25 mg kg^{-1} in 2023 following initial fertilisation, reaching Ferralsol norms (5-20 mg kg^{-1}). Phosphorus increased modestly to 2.7 mg kg^{-1} (below typical 5-15 mg kg^{-1}), while potassium dipped to 18.8 mg kg^{-1} (under 30-150 mg kg^{-1}), attributable to fixation by iron and aluminum oxides and gradual microbial release from organic matter. These findings highlight inherent nutrient limitations in post-mining Ferralsols, where low CEC_{eff} exacerbates cation leaching and oxide fixation hampers P and K availability, impeding ecosystem recovery and agricultural productivity. The sharp N decline post-fertilisation emphasises the need for sustained inputs, while modest P gains suggest emerging microbial contributions that could be amplified through management. For future site development, the following soil management strategies are recommended:

- Liming to pH 6.0-6.5 will enhance CEC_{eff} and unlock fixed nutrients.
- Annual organic amendments (e.g., 5-10 t ha^{-1} compost) can boost SOC, stabilising fertility long-term.

- For agricultural use, balanced NPK fertilizers (e.g., 15-15-15 at 200 kg ha^{-1} per cycle) paired with legume intercropping for biological N fixation will optimize yields while minimizing losses on these low-CEC soils.
- Early implementation during recultivation prevents further degradation, promoting resilient land use in this high-rainfall environment.

4.1.2 Soil Hydrology and Structure

Soil hydrological analyses indicate ongoing soil structure redevelopment, as evidenced by scattered and heterogeneous values in the wet range of the soil water retention curve mainly determined by secondary soil pores attributable to soils structure mediated by soil biological activity. This variability reflects the substantial disturbance from mining-related soil relocation. Given that soil structure restoration is a slow process typically spanning decades to centuries, such findings are expected in post-mining reclamation. These observations underscore the critical role of focused recultivation strategies prioritising soil structure recovery to enhance water infiltration and retention, aeration, nutrient cycling, and erosion control.

4.1.3 Soil Organic Carbon Quality and Climate Change Mitigation

SOC quality assessments reveal that active labile carbon pools (CWSC, HWSC, and POXC fractions), which represent easily decomposable carbon, constitute a low share (3.2–3.9%) of total SOC. This low proportion indicates a dominance of stable carbon pools that favour long-term carbon sequestration, a positive outcome for climate change mitigation. The total SOC gain of 87 t ha^{-1} signifies a strong soil carbon sink induced by recultivation. After three years of recultivation, the average carbon stock at the test site is estimated at 87.6 t ha^{-1}, or 140.16 t SOC across the entire site highlighting the significant potential of optimised recultivation approaches to enhance soil protection and contribute to climate change mitigation. Integrated soil conservation by agroforestry or conservation agriculture could improve climate change mitigation by the recultivated soils with the co-benefit of sustaining long-term fertility and agricultural productivity (Kumar, et al., 2025).

4.1.4 General Conclusions and Future Directions

The cassava planting system has demonstrated significant potential for both soil recultivation and climate change mitigation, as evidenced by increased SOC – paired with the dominance of fractions belonging to the stable carbon pool – and effective reduction of soil water erosion. These findings underscore cassava's role as a robust, low-input option for restoring degraded post-mining landscapes. To build on these results, future research should additionally include biodiversity assessments, which were not addressed in the present study but are critical for evaluating ecosystem recovery and resilience.

As with any agricultural trial, the initial cultivation phase often reveals unforeseen challenges. It is therefore essential to evaluate performance over multiple growing seasons, allowing for iterative refinement of methods and the achievement of optimal outcomes. However, this was not possible in this study as the second cassava planting was destroyed by virus infection and heavy monsoon. As a consequence, further pilot experiments would help to align these findings. While this study focuses on ecological and technical aspects, economic considerations – such as cost-benefit analyses and market integration—will be vital for developing comprehensive, scalable recultivation strategies. Moving forward, long-term monitoring and adaptive management will be key to ensuring the sustainability and success of post-mining land restoration efforts.

4.2 Environmental Impact

Post-mining sites often exhibit elevated concentrations of trace metals in the soil due to residual mining materials, especially from ores. Since trace metals are persistent environmental contaminants, preventing their spread is of utmost importance. A particularly critical aspect is avoiding an increase in the volume of contaminated material, such as soil.

At the experimental site, trace metal concentrations have shown no significant decrease over time, which is a positive indication that these metals are not dispersing in the surrounding environment. Furthermore, the minimal uptake of trace metals by cassava biomass corroborates the strong adsorption and retention of these contaminants within the soil matrix.

Currently, there is no evidence of environmental impact caused by trace metal dispersion under the site's prevailing conditions. All measured trace metal concentrations remain well below regulatory threshold values, further supporting this conclusion. To assess groundwater risk, field- and laboratory-derived trace metal mobilities were multiplied by annual seepage to estimate potential TM loads (Figure 23). For instance, German environmental legislation defines maximum allowable annual TM loads in Annex 1 of the Federal Soil Protection and Contaminated Sites Ordinance of Germany (BBodSchV, 2021). In all cases, estimated annual loads remained far below these limits of 35, 300, 200, and 1,200 g ha^{-1} yr^{-1} for As, Cu, Pb, and Zn, respectively. Highest relative loads were obtained from field-based mobility data, which better represent natural conditions. Even in this conservative scenario, Pb, Cu, Zn, and As loads remained negligible. Moreover, since the groundwater level lies deeper than 10 m, additional retention processes within the vadose zone are expected to further attenuate fluxes prior to water table recharge (El-Aassar, et al., 2023).

However, soil chemical conditions could change, especially with ongoing acidification, potentially mobilising trace metals and facilitating their environmental dispersion. Therefore, although no immediate environmental risks from trace metals are expected at present, the situation warrants continued monitoring to detect and mitigate any future changes in soil chemistry that could alter their mobility.

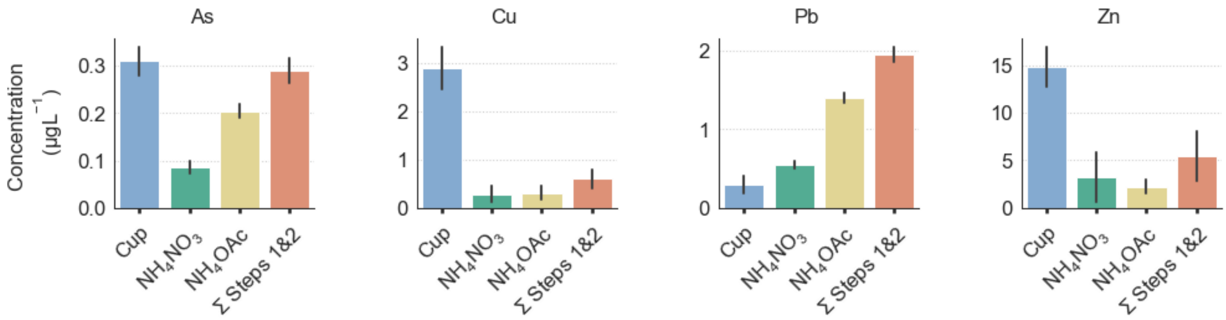

Figure 23: Calculated annual loads of trace metals derived by multiplying the field- and lab-determined mobilities (cf. Figure 2) with the annual cumulative seepage water simulated for 2023.

5 Conclusions

This study demonstrates that post-mining soil recultivation significantly influences soil quality and climate change mitigation potential, as evidenced by increased SOC, low share of labile soil carbon fractions, and effective reduction of water-induced soil erosion. These outcomes highlight the importance of selecting recultivation strategies that foster long-term soil structure recovery and carbon sequestration.

The persistence of trace metals in the soils, while currently stable and below regulatory thresholds, underscores the necessity for ongoing monitoring given the potential for mobilisation under changing soil chemical conditions such as acidification.

Overall, the cassava planting systems not only accelerate soil restoration but also contribute effectively to greenhouse gas mitigation through soil carbon storage and the option to use the cassava tubers for ethanol production to substitute fossils. This aligns with broader sustainability objectives and confirms the potential of targeted recultivation to rehabilitate degraded post-mining landscapes while supporting climate goals.

Future research should incorporate biodiversity assessments and economic evaluations to provide a holistic understanding of recultivation outcomes and optimize land management practices in post-mining contexts.

Literature

Angon, P. B. et al., 2024. Sources, effects and present perspectives of heavy metals contamination: Soil, plants and human food chain. *Heliyon,* April, Volume 10, p. e28357.

Baumgartl, T., Bucka, F., Pihlap, E. & and Filipovic, V., 2023. How do mine rehabilitation strategies affects soil heterogeneity and structure in the long term?. *EGU General Assembly 2023*.

BBodSchV, 2021. *Bundes-Bodenschutz- und Altlastenverordnung vom 9. Juli 2021 (BGBl. I S. 2598, 2716) [Federal Soil Protection and Contaminated Sites Ordinance].* Berlin: German Federal Mininstry for the Environment, Climate Action, Nature Conservation and Nuclear Safety (BMUKN).

Blažka, P. & Fischer, Z., 2014. Moisture, water holding, drying and wetting in forest soils. *Open Journal of Soil Science,* Volume 04, p. 174–184.

Brömme, K. et al., 2018. *Cultivation of energy crops on former mining sites on a pilot scale in Vietnam.* Berlin/Hanoi: Independent Institute for Environmental Issues – UfU.

Chuenchum, P., Xu, M. & Tang, W., 2020. Predicted trends of soil erosion and sediment yield from future land use and climate change scenarios in the Lancang–Mekong River by using the modified RUSLE model. *International Soil and Water Conservation Research,* September, Volume 8, p. 213–227.

Culman, S. W. et al., 2012. Permanganate oxidizable carbon reflects a processed soil fraction that is sensitive to management. *Soil Science Society of America Journal,* March, Volume 76, p. 494–504.

Cuong, L. V. et al., 2025. Variability in soil carbon and nitrogen storage across a chronosequence of Pinus Kesiya plantations in the central highland, Vietnam. *Applied Ecology and Environmental Research,* Volume 23, p. 5041–5059.

DIN EN ISO 11274, 2014. *Soil quality – Determination of the water-retention characteristic – Laboratory methods (ISO 11274:1998 + Cor 1:2009); German version EN ISO 11274:2014.* Berlin(Germany): Beuth Verlag.

El-Aassar, A.-H.et al., 2023. Integration of groundwater vulnerability with contaminants transport modeling in unsaturated zone, case study El-Sharqia, Egypt. *Environmental Monitoring and Assessment,* May.Volume 195.

Feddes, R. A., Kowalik, P. J. & Zaradny, H., 1978. *Simulation of field water use and crop yield.* Wageningen: Centre for Agricultural Publishing and Documentation.

García-Gutiérrez, C., Pachepsky, Y. & Martín, M. Á., 2018. Technical note: Saturated hydraulic conductivity and textural heterogeneity of soils. *Hydrology and Earth System Sciences,* July, Volume 22, p. 3923–3932.

Ha, P. Q., 2010. *Carbon in Vietnamese soils and experiences to improve carbon stock in soil.* Bogor, s.n.

Ha, P. T. et al., 2023. Quantitative exploration of the innovative trend method for evapotranspiration and its sensitivity to climatic variables: The case study of Southeast Vietnam. *Earth Science Informatics,* November, Volume 17, p. 299–314.

Hareesh, P. S., Resmi, T. R., Sheela, M. N. & Makeshkumar, T., 2023. Cassava mosaic disease in South and Southeast Asia: current status and prospects. *Frontiers in Sustainable Food Systems,* June.Volume 7.

He, N. P. et al., 2011. Grazing intensity impacts soil carbon and nitrogen storage of continental steppe. *Ecosphere,* January, Volume 2, p. art8.

Hoang, L. et al., 2024. Vietnamese cassava varieties progression across 50 years. *Ministry of Science and Technology, Vietnam,* March, Volume 66, p. 59–76.

Hoang, N. et al., 2019. Pleistocene basaltic volcanism in the Krông Nô area and vicinity, Dac Nong Province (Vietnam). *Journal of Asian Earth Sciences,* September, Volume 181, p. 103903.

Hurisso, T. T. et al., 2016. Comparison of permanganate-oxidizable carbon and mineralizable carbon for assessment of organic matter stabilization and mineralization. *Soil Science Society of America Journal,* September, Volume 80, p. 1352–1364.

IUSS Working Group WRB, 2022. *World Reference Base for Soil Resources. International coil classification system for naming soils and creating legends for soil maps.* Vienna(Austria): International Union of Soil Sciences (IUSS).

Kumar, A., Antoniella, G., Blasi, E. & Chiti, T., 2025. Recent advances in regenerative sustainable agricultural strategies for managing soil carbon and mitigating climate change consequences. *CATENA,* October, Volume 258, p. 109208.

Le, D. P. et al., 2019. *Characterization of Cassva Production Systems in Vietnam,* Hanoi: s.n.

Miller, G. L., 1959. Use of Dinitrosalicylic Acid Reagent for Determination of Reducing Sugar. *Analytical Chemistry,* March, Volume 31, p. 426–428.

Mwamba, S. et al., 2021. Physiological and Morphological Responses of Cassava Genotypes to Fertilization Regimes in Chromi-Haplic Acrisols Soils. *Agronomy,* August, Volume 11, p. 1757.

National Oceanic and Atmospheric Administration (NOAA), Office for Coastal Management, 2022. *QNSPECT - QGIS Plugin for NOAA Nonpoint Source Pollution and Erosion Comparison Tool (NSPECT).* s.l.:s.n.

Office for Coastal Management, 2024. *Coastal Change Analysis Program (C-CAP) -Regional Land Cover Classification Scheme.* s.l.:s.n.

Orji, O. U. et al., 2021. Assessment of levels and health risks of trace metals in soils and food crops cultivated on farmlands near Enyigba mining sites, Ebonyi State, Nigeria. *Journal of Food Protection,* August, Volume 84, p. 1288–1294.

Panagos, P. et al., 2017. Global rainfall erosivity assessment based on high-temporal resolution rainfall records. *Scientific Reports,* June.Volume 7.

Panagos, P. et al., 2023. Global rainfall erosivity database (GloREDa) and monthly R-factor data at 1 km spatial resolution. *Data in Brief,* October, Volume 50, p. 109482.

Pham, T. T. H. et al., 2018. Study on the environmental state in Tan Rai bauxite mining area Bao Lam district, Lam Dong province. *Journal of Vietnamese Environment,* August, Volume 9, p. 240–247.

Phoncharoen, P. et al., 2019. Growth rates and yields of cassava at different planting dates in a tropical savanna climate. *Scientia Agricola,* October, Volume 76, p. 376–388.

Phuong, T. K., 2015. *Vietnam: Inititial economic effect of bauxite projects in highland.* s.l., s.n.

QCVN 03:2023/BTNMT, 2023. *National Technical Regulation on Soil Quality.* Hanoi: Ministry of Natural Resources and Environment.

Roberto Baizi e Silva, A., 2025. Micronutrients for Production and Biofortification of Cassava. In: H. Wang, ed. *Root Vegetables - Scientific Research and Practical Application [Working Title].* s.l.:IntechOpen.

Sanderman, J. et al., 2017. Greater soil carbon stocks and faster turnover rates with increasing agricultural productivity. *SOIL,* January, Volume 3, p. 1–16.

Sayyadi, S. et al., 2025. Observation-based analysis of groundwater storage in Vietnam's Central Highlands: influence of hydro-climatic variability. *Hydrological Sciences Journal,* October, Volume 70, p. 2993–3012.

Silva, R. M. d. et al., 2023. Measurement of dry matter and starch in modern cassava genotypes during long harvest cycles. *Horticulturae,* June, Volume 9, p. 733.

Šimůnek, J., van Genuchten, M. T. & Šejna, M., 2008. Development and applications of the HYDRUS and STANMOD software packages and related codes. *Vadose Zone Journal,* May, Volume 7, p. 587–600.

Singer, M. B. et al., 2021. Hourly potential evapotranspiration at 0.1° resolution for the global land surface from 1981-present. *Scientific Data,* August.Volume 8.

Singh, P. D. et al., 2023. Possibility of spatial estimation of soil erosion using Revised Universal Soil Loss Equation model and generalized additive model in post-hard coal mining spoil heap. *Land Degradation & Development,* October, Volume 35, p. 923–935.

Swedish Environmental Protection Agency, 2002. *Methods for inventories of contaminated sites.* Stockholm: Swedish Environmental Quality Criteria.

Tran, T. V., Tran, D. X. & Nguyen, D. B., 2023. Agricultural drought in the Vietnamese Central Highlands at 1-km resolution: Monthly and annual datasets. *Data in Brief,* June, Volume 48, p. 109194.

Trinh, M. V., 2007. *Soil erosion and nitrogen leachjing in northern Vietnam: Experimentationa nd modelling,* Wageningen: s.n.

U.S. Department of Agriculture, Soil Conservation Service, 1986. *Urban Hydrology for Small Watersheds.* Washington DC: U.S. Government Printing Office.

Wangpor, J. et al., 2017. Bioethanol production from cassava starch by enzymatic hydrolysis, fermentation and ex-situ nanofiltration.. *Energy Procedia,* October, Volume 138, p. 883–888.

Wischmeier, W. H. & Smith, D. D., 1978. *Predicting Rainfall Erosion Losses: A Guide to Conservation Planning.* s.l.:U.S. Department of Agriculture, Agricultural Research Service.

Zeien, H. & Brümmer, G. W., 1989. *Chemische Extraktion zur Bestimmung von Schwermetallbindungsformen in Böden [Chemical extraction for determining trace metal binding forms in soils].* s.l., s.n., pp. 505-510.

Zou, X. M. et al., 2005. Estimating soil labile organic carbon and potential turnover rates using a sequential fumigation–incubation procedure. *Soil Biology and Biochemistry,* October, Volume 37, p. 1923–1928.